

# Fermilab

Large low background kTon-scale liquid argon time projection chambers

FERMILAB-PUB-23-050-ND

Fermilab Accepted Manuscript

This manuscript has been authored by Fermi Research Alliance, LLC  
under Contract No. DE-AC02-07CH11359 with the U.S. Department of Energy,  
Office of Science, Office of High Energy Physics.

# Large low background kTon-scale liquid argon time projection chambers

T Bezerra<sup>1</sup>, A Borkum<sup>1</sup>, E Church<sup>2,\*</sup>, Z Djurcic<sup>3</sup>,  
J Genovesi<sup>4</sup>, J Haiston<sup>4</sup>, C M Jackson<sup>2</sup>, I Lazanu<sup>5</sup>,  
B Monreal<sup>6</sup>, S Munson<sup>2</sup>, C Ortiz<sup>7</sup>, M Parvu<sup>5</sup>, S J M Peeters<sup>1</sup>, D  
Pershey<sup>7</sup>, S S Poudel<sup>2</sup>, J Reichenbacher<sup>4</sup>, R Saldanha<sup>2</sup>, K  
Scholberg<sup>7</sup>, G Sinev<sup>4</sup>, S Westerdale<sup>8</sup> and J Zennaro<sup>9</sup>

<sup>1</sup> University of Sussex, Brighton, BN1 9RH, United Kingdom

<sup>2</sup> Pacific Northwest National Laboratory, Richland, WA 99352, United States of America

<sup>3</sup> Argonne National Laboratory, Argonne, IL 60439, United States of America

<sup>4</sup> South Dakota School of Mines and Technology, Rapid City, SD 57701, United States of America

<sup>5</sup> University of Bucharest, Bucharest, Romania

<sup>6</sup> Case Western Reserve University, Cleveland, Ohio OH-44106, United States of America

<sup>7</sup> Duke University, Durham, NC 27708, United States of America

<sup>8</sup> Princeton University, Princeton, NJ 08544, United States of America

<sup>9</sup> Fermi National Accelerator Laboratory, Batavia, IL 60510, United States of America

E-mail: eric.church@pnnl.gov and christopher.jackson@pnnl.gov

Received 30 January 2023

Accepted for publication 13 March 2023

## Abstract

We find that it is possible to increase sensitivity to low energy physics in a third or fourth Deep Underground Neutrino Experiment (DUNE)-like module with careful controls over radiopurity and targeted modifications to a detector similar to the DUNE Far Detector design. In particular, sensitivity to super-nova and solar neutrinos can be enhanced with improved MeV-scale reach. A neutrinoless double beta decay search with  $^{136}\text{Xe}$  loading appears feasible. Furthermore, sensitivity to Weakly-Interacting Massive Particle (WIMP) Dark Matter becomes competitive with the planned world program in such a detector, offering a unique seasonal variation detection that is characteristic of the nature of WIMPs.

Keywords: neutrinos, DUNE, module, dark matter, solar neutrinos, supernovae

\* Author to whom correspondence should be addressed.  
<https://doi.org/10.1088/1361-6471/acc394>

(Some figures may appear in colour only in the online journal)

## 1. Introduction

In this study, we introduce and discuss a dedicated low background module that would enhance the physics program of next-generation experiments such as the planned Deep Underground Neutrino Experiment (DUNE). Such a low background DUNE-like module could be installed as either module 3 or module 4, the so-called ‘Module of Opportunity’ in DUNE. Such a module would increase the physics reach of supernova and solar neutrino physics, and could potentially host a next-generation neutrinoless double beta decay ( $0\nu\beta\beta$ ) or Weakly interacting massive particle (WIMP) dark matter (DM) search. We refer to this design as the Sanford Underground Low background Module (SLoMo).

The physics reach would be enhanced by lowering the nominal energy threshold of a DUNE-like experiment from the anticipated 5–10 MeV to levels necessary to address three potential physics targets, as indicated in figure 1, listed in order of increasing difficulty:

- $\sim 3.5$  MeV energy threshold. This threshold is set by the  $Q$ -value of the  $^{42}\text{K}$  (daughter of  $^{42}\text{Ar}$ ) in the detector target. By reducing neutron captures, alpha-emitting radon daughters and pileup events above this threshold, supernova burst neutrino sensitivity could be increased in distance, energy and time. Sensitivity to solar neutrinos would also be enhanced, allowing explorations of interesting solar-reactor oscillation tensions and non-standard interactions.
- $\sim 0.5$  MeV energy threshold. This threshold is set by the decay  $Q$ -value of the  $^{39}\text{Ar}$  in the detector target. With reduction of electron and photon backgrounds in the target, particularly if the  $^{42}\text{Ar}$  content is reduced through the use of underground argon (UAr), sensitivity to low-energy solar neutrinos from the CNO process would allow a precision measurement to be made. Such a detector will be sensitive to  $0\nu\beta\beta$  search with loading of  $^{136}\text{Xe}$ .
- $< 100$  keV energy threshold. This threshold could be achieved by enhancing the light collection within the detector and by lowering the  $^{39}\text{Ar}$  background by deploying UAr. With rejection of electron recoil backgrounds (using timing-based pulse shape discrimination), a sensitive WIMP dark matter search could take place, and interesting phenomena such as a supernova coherent elastic neutrino–nucleus scattering signal (a  $\text{CE}\nu\text{NS}$  glow) could be studied.

These low background targets are achievable due to the unprecedented size and also the increased radiopurity of the module, allowing significant fiducialization and hence less stringent radioactive background requirements than current world-leading dark matter searches. The light enhancements are achievable with current production techniques. As described in section 2.2.3, production of UAr at the scale required for a DUNE module is potentially achievable, though it requires a dedicated effort to identify the potential argon source and work with commercial gas suppliers

In this paper, in section 2, we outline the design of the module and discuss potential paths to achieve the detector requirements. In section 3 we present our initial studies of physics reach of this detector.

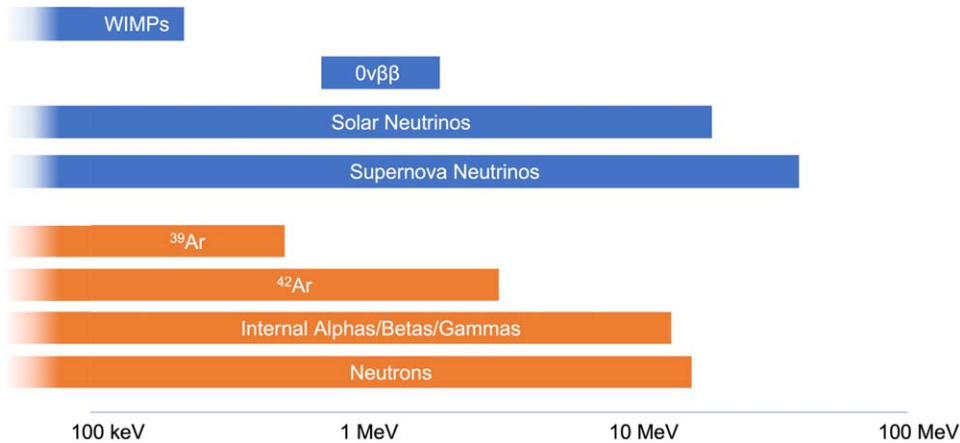


**Figure 1.** Summary of physics targets of this low background module and the primary radiological backgrounds.

## 2. Detector design

This section outlines the proposed design for the low background module and describes in detail the radioactive background control and photon detection system enhancements required to enable physics measurements outlined in the introduction. We note this module design is not necessarily endorsed by the DUNE collaboration, as the so-called ‘Phase II’ process that includes building the final two far detector modules is in its early stages.

### 2.1. Module layout

A low background module and its attendant physics goals are enabled most simply by minimizing the detector components in the bulk of the argon. The resulting module must still allow for very good light detection efficiency and for charge detection efficiency similar to existing designs of large LArTPCs [1–3]. For the benefit of conforming to the longstanding plans for the Long Baseline Neutrino Facility far detector complex and cavern layouts, we also want to use the same commercial cryostat concept and existing module designs to the greatest extent possible and perturb them only where necessary. Starting with the existing DUNE modules, simple modifications assure minimal disruption to the main long baseline neutrino oscillation program to measure the remaining parameters in the Pontecorvo–Maki–Nakagawa–Sakata (PMNS) matrix.

*2.1.1. Single phase.* We therefore, start with DUNE’s Far Detector Vertical Drift Module (VD) [4], sometimes referred to as Module 2, and consider design modifications to suit our low background purposes. We show a working design in figure 2.

Water in ‘bricks’ which are imagined to be nestled among the I-beam support structure achieves large external neutron reduction, as discussed in section 2.2.1. We keep the Charge Readout Planes of the VD unaltered. Similarly, the central cathode of the VD is preserved with the exception that the sparse and mostly distant photon detection modules, known as X-Arapucas, are swapped out for the SiPM modules mounted within the cathode plane—at least on that part of the cathode in the inner region of this detector. An acrylic box of one-inch thickness with  $x, y, z$  extent of 6, 12, 40 m serves to mount SiPM modules and reflective WLS

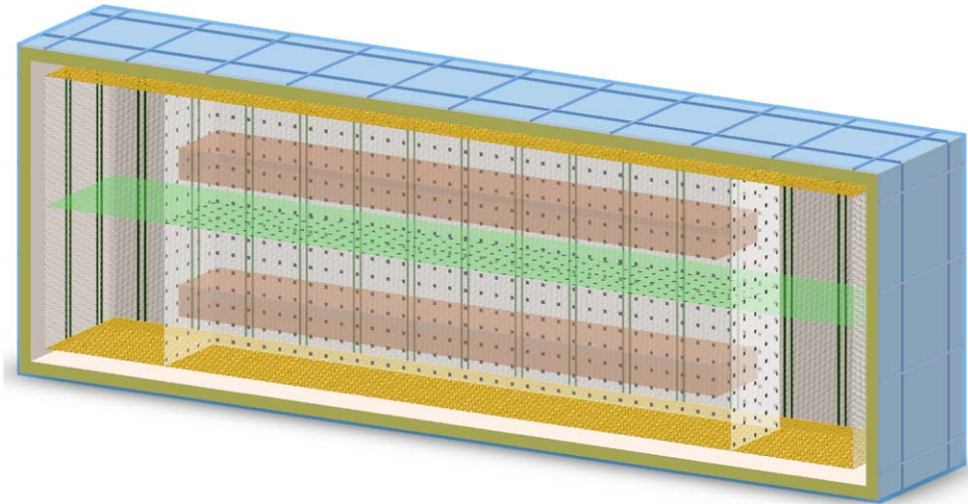


**Figure 2.** Shown is the base design for the proposed low background detector. Blue shows external water ‘bricks’. The top and bottom yellow planes are the Charge Readout Panels unchanged from the Vertical Detector design. The central cathode is in green. The white box of acrylic (full interior volume) is of thickness 1 inch and has  $x$ ,  $y$ ,  $z$  extents of 6, 12, 40 m. The black points are SiPM modules shown here at a coverage of 10%, while some studies in this paper use up to 80% coverage. A proposed fiducial volume totaling 2 kTon is shown in the two beige boxes. This paper also considers a 3 kTon volume.

foils. Here  $x$  is the horizontal dimension,  $y$  is the vertical dimension,  $z$  is in the beam direction. SiPM modules are mounted on the inside of the acrylic box at anywhere from 10% to 80% area coverage. We envision two 1 or 1.5 kTon long skinny fiducial volumes, depending on the study, that has a stand-off of 1.5 m from the central cathode. We also discuss, alternatively, a 3 kTon fiducial volume in this paper in studies where backgrounds from the central cathode are thought to be small or events from it can be reconstructed and cut away.

The bulk volume of this module consists mostly of argon, with only small material contributions such as the slender support structures for the cathode plane panels. As in the VD, there are two 6 m vertical drifts.

## 2.2. Radioactive backgrounds

To enable the physics targets for this module, improvements in control of internal and external radioactive background levels are required. Making a module of this size low background will require significant quality and materials controls beyond what has been attempted by previous experiments, and certainly beyond what is required for the Phase I DUNE program. However, we note that due to the increased size of this module self-shielding in the argon allows the background requirements to be less stringent than those expected to be reached by the current Generation 2 (G2) dark matter experiments. Thus future research and development will need to focus on how to scale the techniques successfully deployed to low background dark matter or neutrinoless double beta decay searches to the kTon scale.

A particular concern for this module will be neutron-induced background events, which will be the main background to the neutrino searches above 3.5 MeV thresholds. A neutron capture in  $^{40}\text{Ar}$  produces a 6.1 MeV gamma cascade which can Compton scatter or pair

produce electrons that can mimic the charged current neutrino interactions in the argon. Captures on  $^{36}\text{Ar}$  can produce 8.8 MeV gamma cascades. Neutrons are also the primary backgrounds for the lowest energy searches for WIMP dark matter, where nuclear recoils can mimic the signal. Below 3.5 MeV the primary backgrounds will come from alpha, beta and gamma emitting isotopes within the argon or detector materials.

*2.2.1. Cavern neutron backgrounds.* The most significant source of neutrons will likely be those induced by spontaneous fission or  $(\alpha, n)$  interactions from the uranium-238 or thorium-232 decay chains within the surrounding rock and shotcrete of the detector cavern. As reported in [5], the external neutron rate at SURF (a likely hosting laboratory for this low background module) is assumed to be  $1.0 \times 10^{-5} \text{ n cm}^{-2} \text{ s}^{-1}$ . As proposed in references [6, 7], it is possible to add water shielding to a DUNE-like cryostat, taking advantage of the space between the structural supports even when the detector is located within a cavern at SURF with limited space around the detector. Those references show that a 40 cm water shield, located within the support structure, is enough to lower the external neutron rate by three orders of magnitude. We assume this is achievable for this module.

The strategy to control the radioactive backgrounds from the detector components such as the cryostat will have three parts:

- improvements to material selection
- additional internal neutron shielding
- and advanced event selections and analysis tools,

with the aim of lowering the internal neutron rate within the detector by at least three orders of magnitude to match the levels of the external rates.

Aside from external neutrons from the cavern, the main source of neutrons in a DUNE-like detector cryostat is likely to be spontaneous fission or  $(\alpha, n)$  interactions from the uranium-238 or thorium-232 decay chains in the order 1 kTon of stainless steel that makes up the I-beam support structure. Research and development will be required to lower the internal background rates by the three orders of magnitude required, for example by careful selection of the raw ingredients and/or control of the manufacturing process. It should be noted that the ‘Generation 2’ dark matter experiments expect to reach neutron rates from their steel a further two orders of magnitude beyond this, so the goal is achievable (even if the scale is much larger than previously attempted). Another area of R&D required to support this goal is improvements in knowledge of  $(\alpha, n)$  cross sections, as highlighted in a recent IAEA workshop [8].

Another approach to reduce neutron background from the internal shielding within the detector would be by adding higher-density rigid polyurethane foam (R-PUF) insulation and/or boron, lithium or gadolinium loaded material layers within the membrane cryostat structure. Our studies show that this could easily reduce the neutron capture rate in LAr by one order of magnitude. One approach, as planned by the DarkSide collaboration, would be to use the additional planes of Gd-doped acrylic to act as a neutron absorber. DarkSide-20k [9] intends to use multiple layers within a ProtoDUNE-style cryostat for their dark matter search. Another design choice might be to take advantage of the existing cryostat but replace some materials such as the insulating foam with a borated version, e.g. to reduce backgrounds from the support structure.

Analysis based cuts can also be used to remove events. For example, with the low threshold of this planned detector, neutron-induced multiple scatters could be tagged and rejected. This takes advantage of the excellent ( $\sim 10$  mm) position resolution of a time projection chamber (TPC). Studies [10] to identify dark matter nuclear recoil backgrounds

show  $\sim 30\%$  reduction at 100 keV threshold and  $\sim 90\%$  reduction at 50 keV, due to the increased probability of detecting an additional scatter at lower thresholds.

*2.2.2. Radon and other internal argon backgrounds.* Radon is an important background that must be controlled as it can diffuse throughout the detector, entering the fiducial volume. The radon decays to a number of daughter isotopes that can be direct backgrounds (for example  $^{214}\text{Bi}$  for a neutrinoless double beta decay search) or that can produce neutrons through  $(\alpha, n)$  interactions. For this low background module we set a radon target level in the liquid argon of  $2 \mu\text{Bq kg}^{-1}$ . This is about three orders of magnitude below the expected DUNE radon level of  $1 \text{ mBq kg}^{-1}$  [11–13].  $2 \mu\text{Bq kg}^{-1}$  has been achieved in liquid argon by the DarkSide-50 experiment [14], and exceeded by DEAP-3600 which achieved a level of  $0.2 \mu\text{Bq kg}^{-1}$  [15]. It should be noted that the higher volume-to-(radon-emanating)-surface ratio in a large detector such as DUNE compared to dark matter detectors will help achieve this target.

To reach this level in a kTon-scale detector will require research and development to implement a combination of the following techniques:

- **Radon removal during purification via an inline radon trap.** No radon removal is in the current design of the purification system for the baseline DUNE. Dark matter and neutrinoless double beta decay search experiments typically use cooled, activated charcoal radon traps to remove radon directly from the recirculating target. The most sensitive dark matter experiments typically purify the argon in the gaseous phase [16, 17], however, such an approach would be impractical for a kTon-scale experiment. Borexino used a charcoal radon trap to purify liquid nitrogen [18], and such an approach could be adopted and scaled appropriately for a low background module. New materials such as Metal-organic frameworks could improve the capture potential beyond charcoal, allowing a potential shrinkage of the footprint of a radon-capture facility to fit the existing cavern designs. Recent evidence from MicroBoone [19] indicates that a copper filter purification system similar to that planned for DUNE may remove greater than 97% or 99.999% of the radon (depending on whether slowed or trapped) in the system without the need for additional removal techniques.
- **Emanation measurement materials campaign.** All materials used in detector construction are known to emanate radon at some level. A large-scale emanation assay campaign to identify materials suitable for construction, similar to the QA/QC campaign described above will be required to ensure the detector can meet the target. A topic for R&D will be how to increase throughput of samples, as emanation measurements typically take two weeks per sample.
- **Surface treatments.** For large components such as the cryostat where it may be impractical and costly to make significant improvements to the radiopurity, surface treatments can be used to lower emanation rates. It is known that acid leaching and electropolishing lowers emanation rates. Coating the inner surface of the cryostat with a radon barrier could lower emanation rates from this significant source.
- **Dust control.** Dust is a significant radon source and cleanliness standards will be higher in this low background module than the baseline DUNE design. Cleanliness protocols and requirements R and D will be necessary to develop automated techniques applicable to the thousands of  $\text{m}^2$ 's of the surface area of a DUNE-like cryostat, for example.
- **Radon reduction system during installation and operation:** the mine air underground is radon laden up to  $1000 \text{ Bq m}^{-3}$  and radon daughter plate-out during installation, filling and operation must be controlled. An upscaled vacuum swing system with large charcoal columns in parallel to remove radon from the ambient air and to provide radon-free air to

the cleanroom and cryostat would be suitable. Vacuum swing systems providing radon-free air have been successfully employed by e.g. Borexino [20], LZ [21] and SuperCDMS [22].

- **Drifting of charged daughters to the cathode.** Several daughters in the radon chain are charged and will drift towards the cathode and out of the fiducial volume. However, this effect may be countered by mixing effects of the purification system.
- **Alpha tagging through pulse shape discrimination.** Alpha events in the radon chain that produce neutrons directly in the argon may be taggable, by identifying the alpha track before the ( $\alpha$ , n) event. Though the amount of light may be relatively small, the timing profile is distinct and may allow pulse shape discrimination on this module with enhanced optical systems.

*2.2.3. Underground argon.* Atmospheric argon (AAr) consists mostly of  $^{40}\text{Ar}$  which is stable. There are some long-lived radioactive isotopes- $^{39}\text{Ar}$  ( $T_{1/2} = 269\text{y}$ ,  $Q_{\beta} = 565\text{ keV}$ ),  $^{37}\text{Ar}$  ( $T_{1/2} = 35\text{d}$ ,  $Q_{\beta} = 813\text{ keV}$ ),  $^{42}\text{Ar}$  ( $T_{1/2} = 32.9\text{y}$ ,  $Q_{\beta} = 599\text{ keV}$ ) [23] which are, in the atmosphere, produced primarily by cosmic ray-induced reactions in  $^{40}\text{Ar}$ . The use of atmospheric argon in a low-threshold multi-ton scale argon detector has limitations due to high  $^{39}\text{Ar}$  activity (1 Bq per kg of argon [24]) in atmospheric argon (AAr). Radiogenic and cosmic-ray muon-induced interactions, especially on K and Ca isotopes, can produce  $^{39}\text{Ar}$  underground. The dominant production channels are negative muon capture on  $^{39}\text{K}$  and ( $\alpha$ , n)-induced (n, p) reactions on  $^{39}\text{K}$ .  $^{39}\text{Ar}$  production underground decreases significantly with depth [25] as muon-flux decreases. DarkSide-50, the only experiment to use underground argon (UAr), measured the  $^{39}\text{Ar}$  activity of  $0.73\text{ mBq kg}^{-1}$  [26], a factor of 1400 smaller than in AAr. With the ARIA project [27], which is planning for a throughput for  $^{39}\text{Ar}$  processing of  $\sim 10\text{ kg d}^{-1}$ , the DarkSide collaboration is planning to further reduce the  $^{39}\text{Ar}$  present in UAr through large-scale isotopic separation by cryogenic distillation.

$^{42}\text{Ar}$  decay in the bulk argon volume will produce  $^{42}\text{K}$  isotopes. While the  $^{42}\text{Ar}$  beta-spectrum has an endpoint of 599 keV, Betas from  $^{42}\text{K}$ -decays span a much larger energy range up to 3.5 MeV, and can be problematic backgrounds. Since UAr should be heavily depleted of  $^{42}\text{Ar}$ , significant suppression of  $^{42}\text{K}$  decay backgrounds is achievable with UAr. In the atmosphere, the  $^{42}\text{Ar}$  concentration is  $\sim 10^{-20}$   $^{42}\text{Ar}$  per  $^{40}\text{Ar}$  atom [28, 29], which is four orders of magnitude smaller than the concentration of  $^{39}\text{Ar}$ . The daughter isotope of  $^{42}\text{Ar}$ ,  $^{42}\text{K}$  ( $T_{1/2} = 12\text{ h}$ ) has two major decay modes: (1) direct beta-decay to the ground state of  $^{42}\text{Ca}$  ( $Q_{\beta} = 3525\text{ keV}$ , BR = 81%), and (2) Beta-decay ( $Q_{\beta} = 2001\text{ keV}$ ) to an excited state of  $^{42}\text{Ca}$  followed by a prompt 1524 keV gamma emission. In the atmosphere,  $^{42}\text{Ar}$  is primarily produced by  $^{40}\text{Ar}$  ( $\alpha$ ,  $2p$ )  $^{42}\text{Ar}$  occurring in the upper atmosphere [29], where energetic alphas are readily available from cosmic-ray muon interactions. Production through two-step neutron capture is also possible but greatly subdominant due to the short-lived intermediate isotope  $^{41}\text{Ar}$  [30]. The  $^{42}\text{Ar}$  production rate underground is not known, but it is expected to be several orders of magnitude smaller than in AAr. Particle interactions on isotopes of K, Ca, and Ti can produce some  $^{42}\text{Ar}$  in the Earth's crust, given the relatively high abundance of the elements (by mass-fraction [31]: K-2.09%, Ca-4.15%, Ti-0.565%). However, the reaction thresholds are high, making  $^{42}\text{Ar}$  production energetically not possible by fission, ( $\alpha$ , n)-neutrons or alphas from the natural radioactivity chains of  $^{238}\text{U}$ ,  $^{235}\text{U}$ , and  $^{232}\text{Th}$ . Energetic particles from cosmic ray muon-induced interactions can produce  $^{42}\text{Ar}$ . But at the depths at which underground argon is usually extracted, the cosmic ray muon-flux should be hugely suppressed, so  $^{42}\text{Ar}$  production should be negligible. Based on GERDA's findings [32], following  $^{42}\text{Ar}$  decays,  $^{42}\text{K}$  nuclei could retain the positive charge long enough to drift in the



influence of electric field. So, we expect  $^{42}\text{K}$  ions to drift and move towards the cathode plane, which suggests an additional suppression of  $^{42}\text{K}$  backgrounds is achievable through fiducialisation.

The  $^{85}\text{Kr}$  isotope, predominantly a  $\beta$ -emitter, has a half-life of 10.7 years and  $Q$ -value of 687 keV [23]. Primary modes of  $^{85}\text{Kr}$  production are spontaneous fission of uranium and plutonium isotopes, neutron capture on  $^{84}\text{Kr}$ , and human-induced nuclear fissions in nuclear reactors [33]. We would expect  $^{85}\text{Kr}$  to be present at some level in UAr. However, its concentration can vary across argon extraction sites. Using the UAr data, DarkSide-50 measured  $^{85}\text{Kr}$  activity of  $2 \text{ mBq kg}^{-1}$  [26], a few orders of magnitude smaller than in AAr.  $^{85}\text{Kr}$  concentration in UAr should also vary depending on the location of the gas reservoir and gas origin (mantle-like or crystal-like). DEAP sees no evidence of  $^{85}\text{Kr}$  in its AAr after filtering in a charcoal trap with 3.3 tonnes of LAr [34].

We expect argon gas extracted from an underground source to be highly depleted of  $^{39}\text{Ar}$ ,  $^{42}\text{Ar}$

and  $^{85}\text{Kr}$ . There is evidence that air-infiltration during the UAr extraction could have contributed to the DarkSide-50's  $^{39}\text{Ar}$ -actual  $^{39}\text{Ar}$  content in the UAr could be significantly smaller (on the order of a few tens of  $\mu\text{Bq kg}^{-1}$ ) [35].  $^{85}\text{Kr}$  and  $^{42}\text{Ar}$  content could also be much smaller. Unlike stable gas isotopes such as  $^{40}\text{Ar}$ , which can collect at gas wells over time, isotopes such as  $^{39}\text{Ar}$  ( $T_{1/2} = 269 \text{ year}$ ),  $^{42}\text{Ar}$  ( $T_{1/2} = 32.9 \text{ year}$ ) and  $^{85}\text{Kr}$  ( $T_{1/2} = 10.7 \text{ year}$ ) diffusing through rocks and collecting in a significant number at the underground gas wells is less likely. However, air-infiltration and cosmogenic activation in the argon bulk could introduce these isotopes in the extracted UAr [36, 37]. Greater care, perhaps, is necessary to ensure avoiding contamination of the UAr during extraction, processing, transport and storage.

While UAr is desirable, it requires a dedicated effort to identify the potential argon source and procure argon on a large enough scale necessary for this project. The Urania plant [9] in southwestern Colorado, USA is expected to produce underground argon from  $\text{CO}_2$  gas wells at a rate of  $\sim 300 \text{ kg d}^{-1}$  (at full rate) for DarkSide. The argon source and the production rate is not large enough for a kiloton scale experiment. The authors are in the process of identifying alternative gas wells with enriched argon streams. Discussions with three potential commercial suppliers are ongoing, however, the underground source samples are not yet tested and low levels of radioactive isotopes must be proven. Initial gas analysis indicates the mantle origin of this sample, with suppressed cosmogenic production compared to a crust source. Based on estimates by the gas suppliers, the production cost could be as low as three times the cost of atmospheric argon and 5 kTon of argon production per year could be achievable.

*2.2.4. Surface storage and spallation issues.* During above-ground storage of our UAr, before placement into the underground module,  $^{39}\text{Ar}$  is produced by cosmogenic neutrons in the reactions:  $^{40}\text{Ar}(n, 2n)^{39}\text{Ar}$  and  $^{38}\text{Ar}(n, \gamma)^{39}\text{Ar}$ . Production cross sections for  $^{39}\text{Ar}$  have been measured in [38].  $^{42}\text{Ar}$  is produced primarily in  $^{40}\text{Ar}(\alpha, 2p)^{42}\text{Ar}$  reactions [29]. In a previous work [39], to which we refer the interested reader, the cross sections for these reactions were obtained from nuclear reaction codes and confronted with data where they exist. An evaluation of cosmogenic  $^{39}\text{Ar}$  and  $^{42}\text{Ar}$  production in UAr stored on the surface can be found in [40]. A full study of expected spallation and pileup backgrounds during the detector operation is in reference [6].

### 2.3. Light collection enhancement

The light collection for this low background module will be enhanced to enable two main goals:

- Lower the energy threshold and improve the resolution at these lower neutrino energies.
- Improve pulse shape discrimination for radioactive background rejection.

In this section, we describe the improvements to the light detection system required to enable this.

*2.3.1. Light collection efficiency impacts on energy resolution.* Charged particles that traverse the liquid argon deposit energy and excite and ionize the argon atoms. This process results in the electrons recombining with the ions generating unstable argon dimers, which decay and emit scintillation light. If an electric field is applied, a fraction of the electrons will drift away before recombining. These ionization electrons are collected by the anode plane and create the charge signal by removing electrons that would have recombined yields an anticorrelation between the light and charge signals observed in LArTPCs. The small number of ionized argon atoms at low energies means that fluctuations in this recombination process can smear the amount of charge observed in energy deposits. The Noble Element Simulation Technique (NEST) collaboration has explored the precision of LArTPC for 1 MeV electrons as a function of charge readout signal-to-noise ratio and the efficiency of collecting light [41]. They predict that using only the charge signal in a LArTPC, the most precise one can reconstruct the energy for a 1 MeV electron is 5% and MicroBooNE has validated this prediction [42]. To improve the energy reconstruction, further one needs to include measurements of scintillation light.

The NEST collaboration explored the expected energy resolution enhancements that a LArTPC can achieve by including light signals along with the charge measurement [41]. Shows that the energy resolution for a 1 MeV electron for LArTPCs with different signal-to-noise ratios (SNR) and varying light collection efficiency. In particular, we see that a LArTPC with SNR near 40 needs 50% of the scintillation light to measure energy deposits with 1% precision.

*2.3.2. Photosensors.* As a baseline design, our plan is to use 24 cm<sup>2</sup>, DarkSide-20k style [9], SiPM tiles. 50% quantum efficiency at visible wavelengths. We assume here another 50% wave length shifter (WLS) efficiency from, e.g. TPB on the tile surface, for a total efficiency of 25%. For maximum light detection we envision covering inside the cathode (between the two planes of cathode wires, as will be done in module 2) and the interior acrylic walls at up to 80% coverage. We assume the Module 2 power-over-fiber concerns [4] to be solved to allow our SiPM coverage of the cathode. The resulting number of SiPM modules for 10% coverage—a value which current studies naively show is sufficient for a dark matter search using pulse shape discrimination—is  $\sim 50\,000$ , to be compared to DarkSide-20k's planned

$\sim 10\,000$ . However, as discussed in section 2.3.1, to achieve the energy resolution required for a neutrinoless double beta decay search will require significantly more coverage. It is likely possible to optimize the placement of the tiles around the fiducial volume, to reduce the total number required, and work is ongoing to study this.

*2.3.3. Reflectors.* To maximize the light capture in this module the surface of the acrylic box will be coated with a reflector to create a light-tight inner volume. If a PTFE reflector is used, as in DarkSide-50, reflectivities of 97% should be possible.

*2.3.4. Argon purity.* The baseline requirement for DUNE is  $<25$  ppm of nitrogen to ensure that photon propagation in the argon is not attenuated. For our simulation studies, we assume that attenuation (absorption) lengths of order 50 m are achievable, which corresponds to nitrogen contamination levels of 1–2 ppm [43]. We note that dedicated dark matter experiments have achieved ppb levels of purity.

### 3. Physics studies

This section outlines the key physics goals of this module and describes the studies that have been performed.

#### 3.1. Argon-39 studies

Reduction of the rate of  $^{39}\text{Ar}$  is desirable for a number of reasons. This 600 keV endpoint beta emitter decays at a  $1 \text{ Bq l}^{-1}$  rate in ordinary atmospheric argon. It may mask low-energy physics by creating optical signals that confuse the reconstruction process. It also represents a serious hurdle in the detector triggering considerations.

Trigger primitives, which constitute a  $6 \text{ PByte year}^{-1}$  data source, not necessarily to be stored into perpetuity, are still an onerous data flow to deal with during steady data-taking. That number drops to far more manageable tens of TBytes if the  $^{39}\text{Ar}$  is reduced by a factor of 1400. In reality, of course, much of the data budget will perhaps be consumed by low-threshold activity in this detector.

Perhaps the more pernicious practical problem is that  $^{39}\text{Ar}$  beta decays may reconstruct as optical ‘hits’ which may, in turn, comprise ‘flashes’ which then confuse the charge-light association for reconstructed physics objects—especially at low energy and far from the light detectors (Hits are simply individual light signals over the threshold and the parameters that characterize them, and flashes are collections of hits in narrow ranges of time, hypothesized to be of the same physical origin). We have performed a study in a Module 1-like environment, not shown here, that gives the not very surprising conclusion that supernova flashes become unambiguously matched with a  $\times 1400$   $^{39}\text{Ar}$  reduction.

Third, the highly desirable property of pulse shape discrimination (PSD) in Argon which would allow to subtract out the nuisance  $^{39}\text{Ar}$  contribution for our, e.g. dark matter search ambitions, is not practicable if pileup is too intense. We show in [10] and discuss later in this paper that a  $\times 1400$  reduction of  $^{39}\text{Ar}$  just allows for a search in our fiducial volume down to 100 keV thresholds and perhaps lower.

Here we mention that even a  $\times 1400$  reduction of  $^{39}\text{Ar}$  does not allow this detector to get to arbitrarily low thresholds for searches of physics with electronic signatures—as opposed to neutron-like interactions. We expect that reductions by this amount will still leave  $^{39}\text{Ar}$  as an overwhelming background to low-rate, low-energy solar processes, for example.

#### 3.2. Simulation

Almost all studies in this paper are carried out in a standalone Geant4 [44] simulation. Source code and build instructions are found at [45]. In that simulation is proper isotope decay and neutron physics, along with optical physics. The volume is basically a 10 kTon box of liquid argon, but with a reasonable model of the cryostat walls on all six sides with charge readout planes (CRPs) made of G10 on the floor and ceiling, as in the VD. Further, there is an acrylic box inside, open on top and bottom and tiled with  $24 \text{ cm}^2$  SiPM modules at an 80% coverage. SiPM modules with that same coverage viewing both upper and lower volumes also tile the

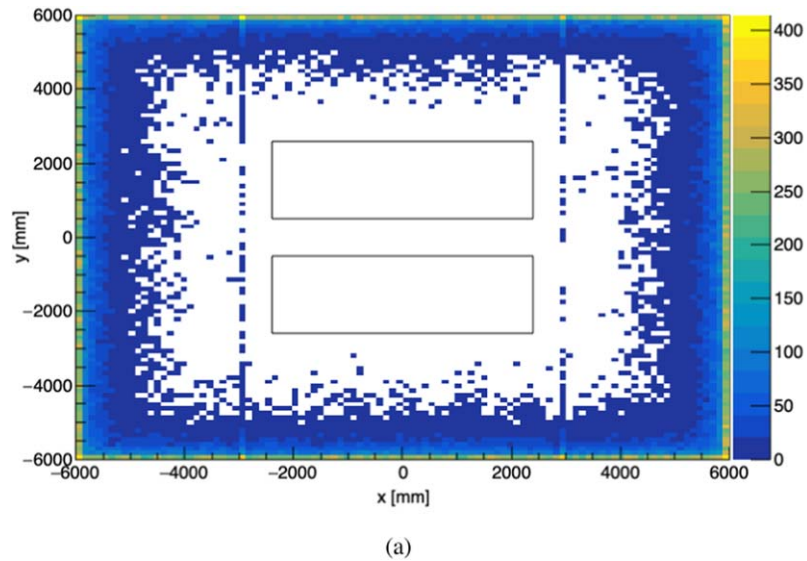


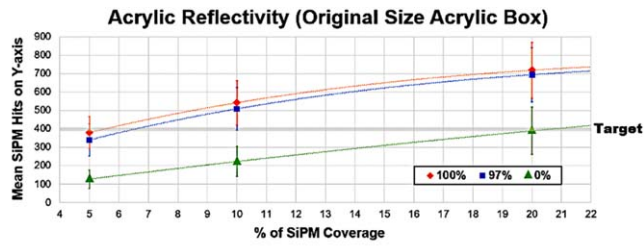
**Figure 3.** Interactions are shown above 100 keV for neutrons emanating from the cold cryostat stainless steel at  $2 \times 10^{-10}$  neutrons  $\text{cm}^{-3} \text{s}^{-1}$  for a 1.4 yr exposure. We show a possible  $\sim 3$  kTon fiducial volume pair, avoiding the cathode, looking down the beamline (The vertical bands are interactions in the acrylic).

central cathode plane. See figure 2 for a representation of our simulated geometry. Figure 3 shows neutron scatter locations where the nuclear recoil energy exceeds 100 keV. We use an after-the-fact 25% total quantum efficiency by merely scaling by that fraction of the detected hits. There is no SiPM electronics response applied. We include a 96% reflectivity of the acrylic surface and a 44% reflectivity for the CRPs (as the holes in each CRP are about 56% of the surface area) and impose an argon attenuation (absorption) length of 50 m, and a Rayleigh scattering length of 90 cm. All simulations generate their 128 nm photons *ab initio* from the charge particles which create them and are propagated on the fly, with no lookup libraries, until their endpoint on a SiPM where they are counted or disappear through absorption.

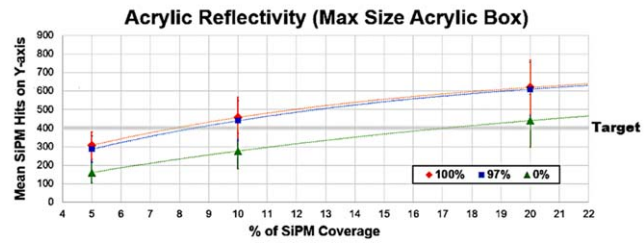
### 3.3. Optical studies

The simulation described in section 3.2 was used to study the minimal requirements for the optical system to allow pulse shape discrimination in a dark matter search, including the required reflectivity of the acrylic box and anode readout surfaces as a function of SiPM tile coverage. The minimal photon counting requirement for the optical system was set at 400 photons reaching the SiPM surface, which results in a total of 100 photons being detected due to the assumed 25% efficiency described in section 2.3.2. The 400 (100) photon requirement was chosen as the minimal amount of photons required to perform a pulse shape discrimination analysis such as that described in section 3.7.

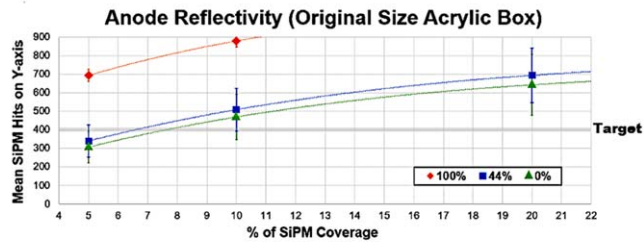
The results of the simulation are shown in figure 4. The studies were performed varying acrylic and anode reflectivity between 0% and 100% (a realistic 97% is highlighted) and then varying the SiPM coverage on the walls and cathode plane to count the accepted photons. Both the standard acrylic box described above and also a maximally sized box where the walls are moved out to the edges of the detector were simulated. This large box would be the



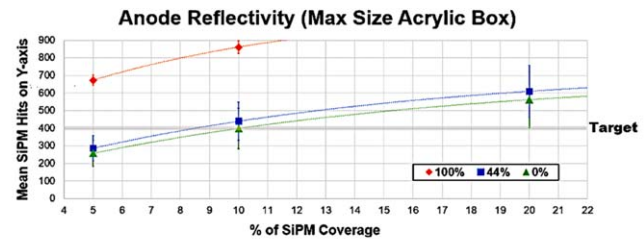
(a)



(b)



(c)



(d)

**Figure 4.** Number of photons detected at the SiPMs as a function of coverage, varying both reflectivity of the surrounding acrylic and anode plane walls, and the size of the acrylic box containing the inner volume, from Original Size ( $6 \times 12 \times 20 \text{ m}^3$ ) to Max Size (at fiducial boundaries at  $12 \times 12 \times 60 \text{ m}^3$ ).

worst-case optics scenario, maximising the path length of the photons. The studies show that a relatively modest amount of SiPM coverage of 10%–20% is required even in the worst-case scenarios to reach the target.

The effect of attenuation with the liquid argon was also studied. Figure 5 shows the number of photons detected at the SiPMs as a function of SiPM coverage for a variety of

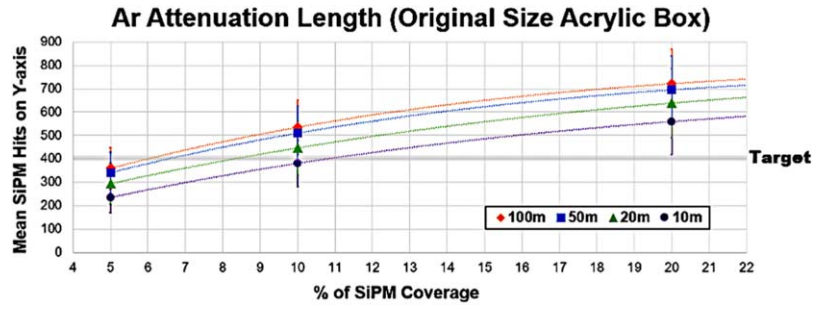


**Figure 5.** Number of photons detected as a function of SiPM coverage when varying the attenuation length within the argon.

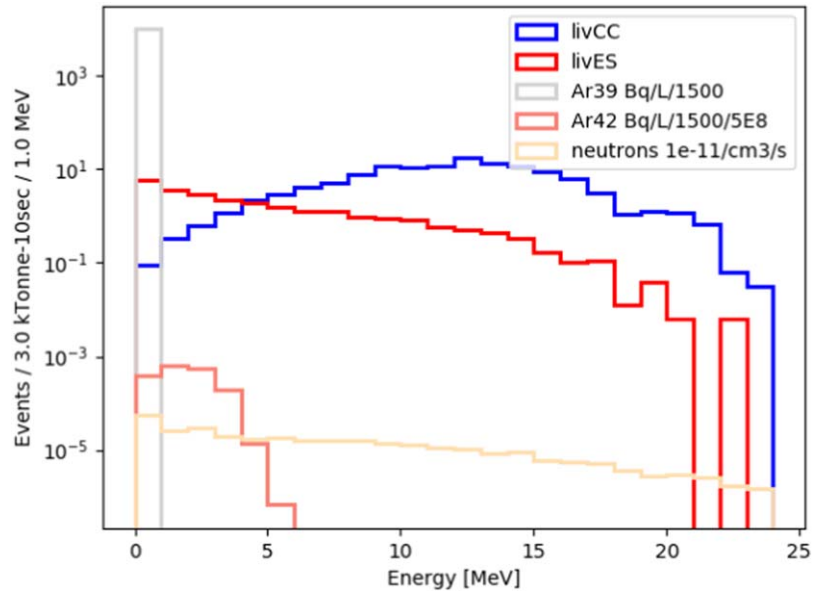


**Figure 6.** Energy deposited from neutrinos from supernova located at 10 kpc, assuming the Livermore model, during a ten-second detector exposure window. Here we presume no Rn222 contribution and a likely too conservative  $\times 500$  Ar<sup>42</sup> suppression in UAr with respect to that achievable in atmospheric argon. Reaching 5 MeV SN detection is straightforward in this module.

different attenuation lengths. Assuming the relation between nitrogen contamination of the argon versus attenuation found in [43], this study shows that the 10%–20% SiPM coverage is sufficient to tolerate 0.5–5 ppm levels of nitrogen within the argon.

### 3.4. Supernova neutrino physics

In this section, we present several supernova neutrino burst studies that could be enhanced by this module. This includes increased sensitivity to lower energies, later times and sources from greater distances. We also discuss the CE $\nu$ NS glow sensitivity.

*3.4.1. Supernova energy spectrum.* We wish to explore the potential improvement provided by a low background large LArTPC to that achievable in current DUNE Far Detector designs for sensitivity to supernova explosion detection. To this end, we simulate a ten-second exposure of our detector to a flux of electron neutrinos from the Livermore [46] supernova model and run them through the MARLEY [47] event generator to produce the final state particles in liquid argon. MARLEY considers all candidate  $\nu_e$  processes, including coherent, elastic, and charged current processes. The detector response is provided by the simulation described in previous section 3.2.

Using that simulation we count SiPM hits for 80% coverage and convert to energy using a simple conversion. That conversion comes from running 3 MeV electrons uniformly through the detector and counting SiPM hits in a coarse  $x, y, z$  binning of the production point. We emphasize that this study is simplified and that refinements including TPC charge response as well as better SiPM energy resolution will result in improvements. Events must originate in the inner 3 kTon fiducial volume. The result is shown in figure 6. The most evident feature is that the elastic scattering component of the  $\nu_e$  flux becomes dominant at low energies inaccessible to the baseline DUNE far detectors—and it does so because neutron rates are required to be low from the cold cryoskin stainless steel and the  $^{42}\text{Ar}$  is at very low levels in UAr. The threshold here can go all the way down to 600 keV, which is a factor of roughly 18 lower than the baseline DUNE far detector design.

The low detector threshold allows access to a significant number of elastic scatter events within the liquid argon. This opens up the possibility of reconstructing the position of the supernova with a pointing analysis. Liquid argon TPCs, with an excellent track resolution, are well suited to making this measurement. With the expected reduction in backgrounds in this sample, a clean elastic scatter sample will dominate at thresholds below 5 MeV (see figure 6), though pointing with these reconstructed tracks is challenging.

*3.4.2. Supernova trigger.* The trigger system in a DUNE-like LAr detector relies on the so-called Trigger Primitives (i.e. hits, TPs) generated from the electronics connected to the wires or photo-sensors. They are simple objects constructed from the signal waveform. A stream of TPs arrives in the trigger module of the DAQ, which will use them to form a Trigger Activity (i.e. a cluster of hits, TAs), which is an association in time and space done by a trigger algorithm. A TA is related to each sub-module/component of the detector (e.g. an APA module), and multiple TAs form a Trigger Candidate (TC). Having a positive TC, the readout system stores the requested data. For low-energy physics, which does not have an external trigger like beam events, it is essential to understand the detector backgrounds (e.g. radiological and electronic noise), to avoid triggers issued by undesired data. Thus, a Low background LAr detector can perform better than the current designs.

The bottleneck for designing efficient supernova neutrino burst (SNB) trigger algorithms is the data transfer and storage resources available for the detector. To get the most of an SNB event, around 100 s of full detector readout is desirable, which means about 150 TB of raw data for a 10 kTon LAr detector. It will take about one hour to transfer the data from this trigger event from the detector caverns to the storage on the surface and several additional hours to transmit those data to the primary storage centre. Therefore, while the effective threshold must be set low enough to satisfy the requirements on SNB detection efficiency, it is crucial to not fire too frequently on background fluctuations. A requirement on the fake trigger rate of once per month is determined by these limits on data-handling, for a DUNE-like LAr detector. Additionally, the triggering decision needs to be made within 10 s since this is the typical amount of data buffered in the DAQ. SNB triggers are likely to be both TPC-and Photon Detection System (PDS)-based in far detector modules one and two, though at the

lower energy thresholds we concern ourselves with in this paper a PDS-only trigger will be required.

In current studies, both TPC and PDS information gives a tagging efficiency of about 20%–30% for a single neutrino interaction [48]. Reducing the estimated neutron capture rate in the LAr volume by a factor of ten (which is the principal background for SNB triggering, given the higher de-excitation gamma energy of about 6 MeV when compared to other radiological components), this efficiency improves to 70%, which translates to a 100% (20%) SNB triggering efficiency for a Milky Way (Magellanic Clouds) SNB. The trigger strategy described above is a ‘counting’ method. If we utilise the integrated charge of each TP, it is possible to construct a distribution of the TAs raw energy (SNB signal with backgrounds) and compare it to the background-only one. The ‘shape’ triggering method improves the efficiency to tag Magellan Clouds’ SNB. The efficiency figure for such an SNB producing ten neutrino interactions (see [48]) shows the efficiency as 70% in a ten kTons DUNE-like LAr detector using the standard DUNE background model described in [1] and a shape triggering algorithm that keeps the fake trigger rate to one per month.

With the Low background LAr detector, a less stringent selection can be used, increasing the signal efficiency while keeping the fake trigger rate at the requirement level. Thus, higher efficiencies will be reached with a lower number of SN events, it then being possible to achieve 100% efficiency to trigger a Magellan Cloud SNB. Identifying Andromeda’s SNBs is more challenging even with this design since they do not produce enough interactions in the whole detector volume in a 10 s window (see the supernova sensitivity plot in [48]), and lowering the TA requirements would encounter the  $^{39}\text{Ar}$  activities.

*3.4.3. Late time supernova neutrinos.* The neutrino flux from a core-collapse supernova is expected to cool over a few tens of seconds, with the late-time events getting lower and lower in energy. The tail end of the burst, where a black-hole formation cutoff may be present, will be challenging to observe. A lower energy threshold extends the time range with which a large liquid argon detector can follow the evolution of the supernova burst [49].

*3.4.4. Pre-supernova neutrino signal.* Another benefit of lowering the threshold is the potential sensitivity to pre-supernova neutrinos [50–56]. The final stages (hours to days) of stellar burning before the core collapse are expected to be associated with an uptick in neutrino production and energy, and observation of these could provide a true early warning of a core-collapse supernova. The pre-supernova flux is expected to be small, and energies are typically less than 10 MeV; nevertheless, they may be observable in a large liquid argon detector with a low threshold [53] for progenitors within a few kpcs nearing the end of their lives.

*3.4.5. CEvNS glow.* Coherent elastic neutrino–nucleus scattering (CEvNS) [57, 58] is a process that occurs when a neutrino interacts coherently with the total weak nuclear charge, causing the ground state nucleus to recoil elastically. The cross section is large compared to the inelastic charged- and neutral-current interactions, but resulting nuclear recoil energies are in the few tens of keV range. CEvNS has now been observed in argon by the COHERENT collaboration using the stopped-pion neutrino flux from the Spallation Neutron Source [59] with a cross section of order  $22 \times 10^{-40} \text{ cm}^2$  for an incoming average flux of  $\langle E_\nu \rangle \approx 30$  MeV from pion decay at rest.

In a large LArTPC there will be a high rate of CEvNS in a core-collapse supernova burst—approximately 30–100 times more events with respect to  $\nu_e$  CC (the dominant inelastic channel), depending on the expected supernova spectrum. However, each event is



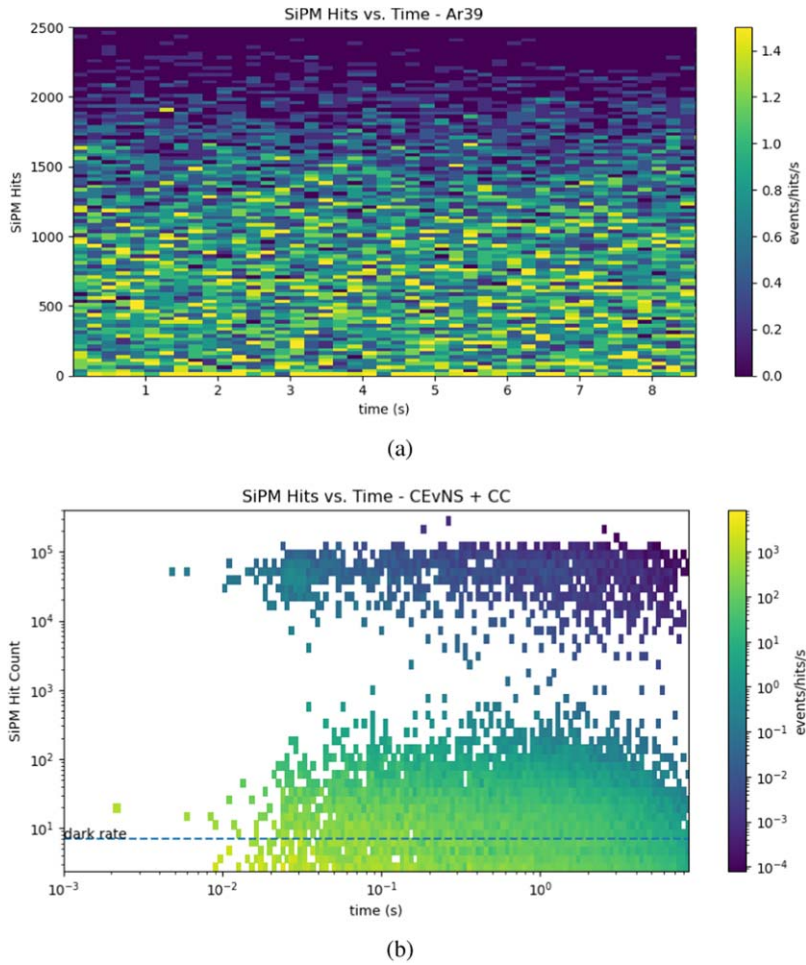


**Figure 7.** The CEvNS glow is the statistically significant increase observed from the low SiPM hit-count CEvNS Supernova events, shown in bottom population of figure (b) that sits on top of the rate of  $^{39}\text{Ar}$  seen in figure (a).

individually not likely to produce more than a few detected photons, and sub-50 keV thresholds need to be achieved to find these events if they are to be found one by one. Even with depleted argon, the  $^{39}\text{Ar}$  rate down in this range in our proposed detector is by far overwhelming. However, an alternative is to identify a ‘CEvNS glow,’ [60] in which the excess rate of detected photons can be tracked statistically above the  $^{39}\text{Ar}$  rate as a function of time in a characteristic explosion. Figure 7 shows that simulated supernova-induced activity from a burst at 10 kpc over 10 s in an inner fiducial 3 kTon gives three distributions: broadly-distributed-in-time, higher-energy charged current (CC) component, a burst of low-hit-multiplicity CEvNS events at about 0.01 s, and then the absolutely flat  $^{39}\text{Ar}$  activity. In ongoing work, we propose to subtract the reconstructed CC events and fit into the CEvNS bump above the background. We note that in principle, an excess of collected ionization from CEvNS events is observable as a ‘CEvNS buzz’ in coincidence with the CEvNS photon glow.

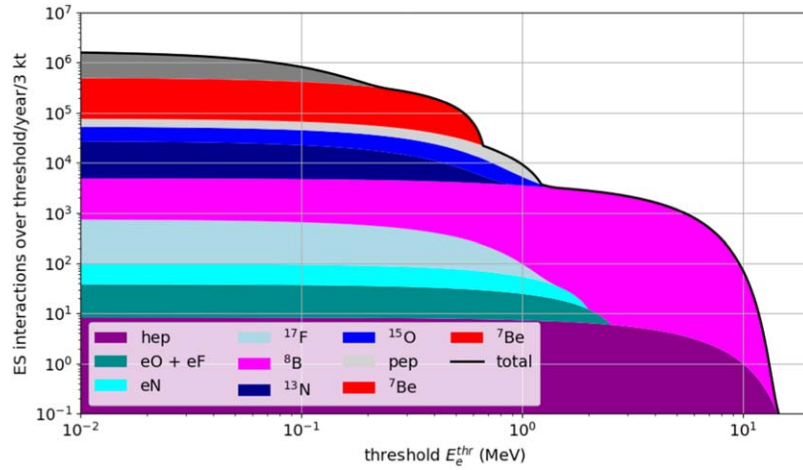


**Figure 8.** Number of events over threshold for solar-neutrino ES interactions in argon for a 3 kTon-year exposure with contributions from different solar fluxes.

### 3.5. Solar neutrino physics

In this section, we present our enhanced sensitivity to solar neutrino searches including lower energies and enhanced oscillation sensitivity to  $\Delta m_{21}^2$ . This allows exploration of solar-reactor oscillation tensions and Non-Standard Interactions. It also allows a precision CNO solar neutrino measurement and a measurement of the  ${}^3\text{He}+p$  solar flux. A first study of DUNE as the next-generation solar neutrino experiment is presented in reference [7]. That study is dominantly one of higher-energy  ${}^8\text{B}$  CC processes, but in this section, we widen the discussion and point out what a lower threshold would offer to solar neutrino studies.

**3.5.1. Low threshold gains and elastic scattering.** Figure 8 shows the number of expected ES interactions over the threshold for a 3 kTon-year exposure. One sees that reducing the threshold to 1 MeV makes *pep* and CNO neutrinos observable. A threshold of 0.5 MeV could add  ${}^7\text{Be}$  neutrinos, and 0.1 MeV could allow for detection of pp neutrinos, though this threshold encroaches into the large  ${}^{39}\text{Ar}$  background, even in UAr. The total number of available neutrinos is important for possible studies discussed in section 3.5.3. This amounts to 9, 200 neutrinos for a 1 MeV threshold, 130 000 neutrinos for a 0.5 MeV threshold, and 820 000 for a 0.1 MeV threshold.

In addition to the previously discussed methods for reducing backgrounds, we are investigating directionality with ES for all solar neutrinos and Cherenkov radiation for more energetic  ${}^8\text{B}$  neutrinos as ways to enhance neutrino signal over backgrounds.

**3.5.2. Solar neutrino oscillations.** Current measurements of the neutrino mixing parameter,  $\Delta m_{21}^2$ , using solar neutrinos from SNO and Super-Kamiokande are currently discrepant at  $1.4\sigma$  with measurements from KamLAND using neutrinos from nuclear reactors [61]. Differing results from these two methods would suggest new physics possibly involved with exotic matter effects as the neutrino passes through the Sun and Earth. Further data from DUNE will further investigate this discrepancy with high statistical significance. The sensitivity comes from the ‘day-night’ effect, a partial regeneration of the  $\nu_e$  solar flux due to

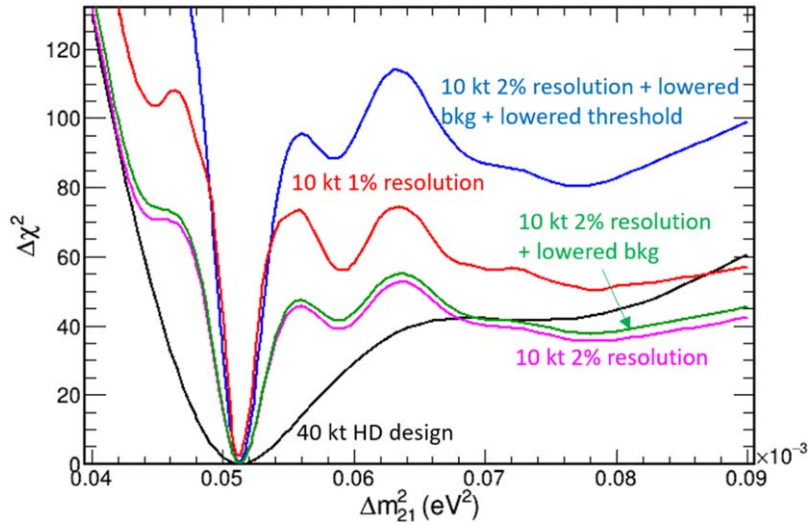


**Figure 9.** Sensitivity of a low-background module to the neutrino mixing parameter  $\Delta m_{21}^2$  assuming a true value of the solar best fit,  $5.13 \times 10^{-5} \text{eV}^2$  [61]. Colored contours show sensitivity after  $100 \text{ kTon yrs}^{-1}$  for various detector configurations compared to  $400 \text{ kTon yrs}^{-1}$  of DUNE data with horizontal drift design, shown in black and dominated by CC events.

matter effects in Earth which depends on  $\Delta m_{21}^2$ , neutrino energy, and nadir angle. This is an advantageous strategy allowing for constraints of uncertainties using daytime data.

Solar neutrinos are much lower energy than typically observed in DUNE making reconstruction of these events challenging. Also, at these low energies, radiological backgrounds, principally neutron capture with a contribution from  $^{40}\text{Ar}$  ( $\alpha$ ,  $\gamma$ ), dominate analysis backgrounds. A low-background DUNE-like module with enhanced light collection will help with both of these challenges.

Improved energy resolution from increased photodetector coverage would significantly improve DUNE-like sensitivity to  $\Delta m_{21}^2$ . This would both improve the reconstruction of the dominant neutron background around the 6.1 MeV total visible energy of the neutron capture on argon-40, and better measure the dependence of the  $\nu_e$  flux regeneration on neutrino energy. A single 10 kTon, a low-background module could discern between SNO/SK and KamLAND best fits at over  $6\sigma$ . Lower neutron background levels would also improve the signal-to-background ratio for the measurement, which could also lower the energy threshold

for detecting and analyzing solar neutrino events. An estimate of sensitivity to  $\Delta m_{21}^2$  with  $100 \text{ kTon yrs}^{-1}$  of exposure with a low-background module is compared to DUNE's sensitivity with  $400 \text{ kTon yrs}^{-1}$  of data from nominal, horizontal drift modules in figure 9. We use a larger 10 kTon fiducial volume for the reduced background/threshold curves in that figure, increased from other studies in this paper.

**3.5.3. Non-standard neutrino interactions.** Non-standard neutrino interactions (NSI) could modify neutrino oscillations in the Sun and result in a different number of neutrinos observed compared to the one predicted by the Standard Model [62] (see also studies with different parameter definitions in [63] and [64]).

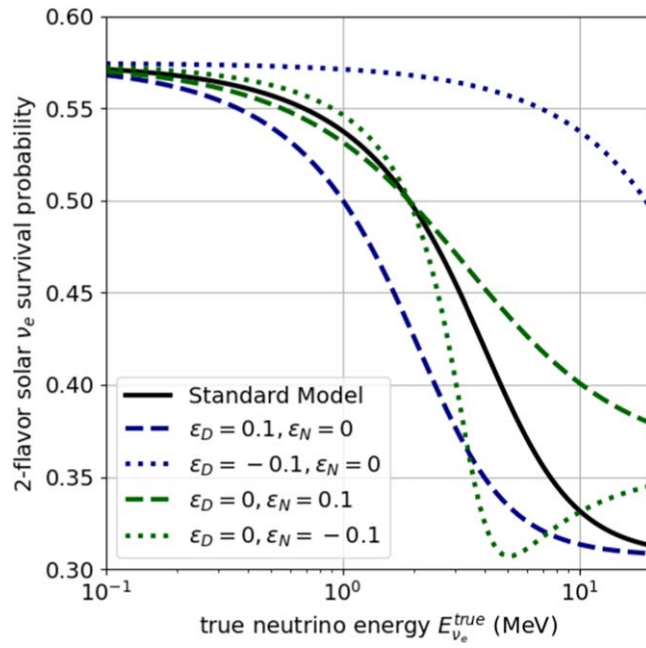


**Figure 10.** 2-flavor electron-neutrino survival probability for solar neutrinos for the Standard Model and several different NSI couplings.

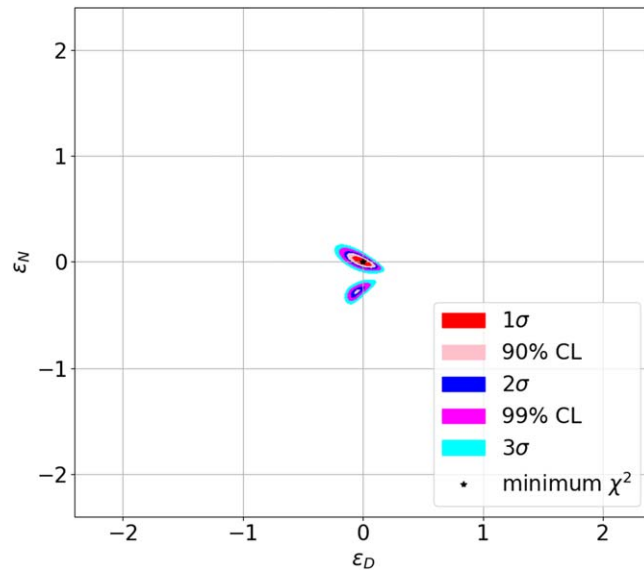


**Figure 11.** Possible NSI constraints for 3 kTon years obtained with the proposed module.

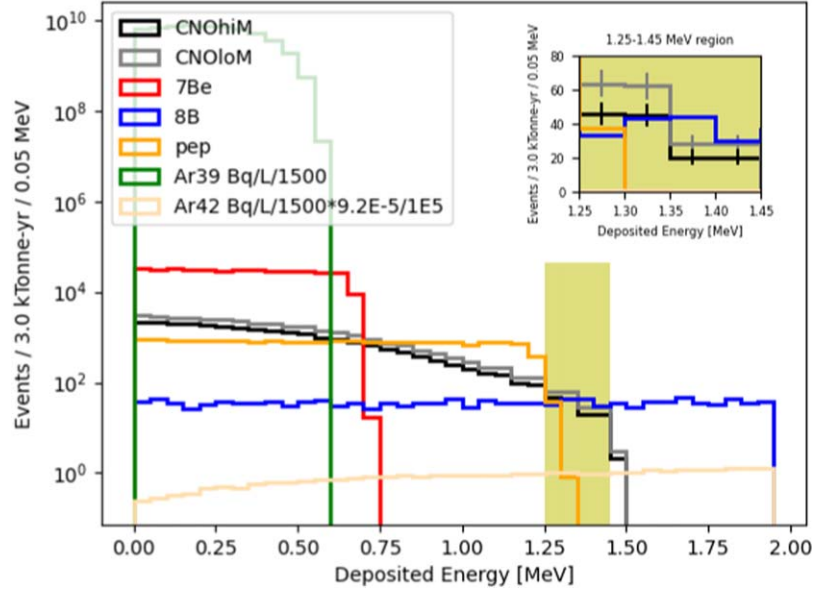


**Figure 12.** CNO solar neutrinos with backgrounds taking radon to be solved and negligible and neutrons constrained. This is 2% smeared true deposited energy in our inner 3 kTon fiducial volume in a year. Note that a likely, low  $^{42}\text{Ar}$  level is shown that reveals that a CNO fit is possible above the  $^7\text{Be}$  peak and explicitly by a simple counting experiment in roughly the region shown in yellow. This is a lower  $^{42}\text{Ar}$  level than shown in figure 1, but still realistic. The inset zooms in on the 1.25–1.45 above the *pep* region to show that the signal statistics are large enough to favor either high- or low-metallicity after a year.

The NSI Hamiltonian (for neutral currents only) relevant for solar-neutrino oscillations can be written in the following form:

$$H_\nu^{\text{NSI}} = \sqrt{2} G_F (n_u + n_d) \begin{pmatrix} -\epsilon_D & \epsilon_N \\ \epsilon_N^* & \epsilon_D \end{pmatrix}, \quad (1)$$

where  $G_F$  is the Fermi constant,  $n_u$  and  $n_d$  are the up- and down-quark densities, respectively, and  $\epsilon_D$  and  $\epsilon_N$  are the diagonal and off-diagonal NSI couplings. These couplings affect  $\nu_e$  solar survival probability (see figure 10). The diagonal coupling can mimic different vacuum  $\Delta m^2$  values, resulting in its incorrect measurement when NSI are not taken into account.

Detection of ES in the proposed module (see section 3.5.1) allows for a great opportunity to have an almost NSI-independent anchor point in the oscillation probability near 0.1 MeV in addition to investigating NSI in solar-neutrino oscillations at several MeV energies where changes in oscillation probability could be large but not much experimental data exists, yet.

An example of possible constraints on the NSI couplings is shown in figure 11. This plot was obtained with the assumption of no backgrounds or systematic errors, an energy threshold of 1 MeV, and an exposure of 3 kTon-years. For comparison, see the larger constraints using current neutrino data available in [61].

**3.5.4. Precision measurement of CNO flux.** The CNO flux has been measured [65] recently by the Borexino collaboration to  $3.5\sigma$  above 0, though it yields indistinct information about the high or low metallicity solution. Per [65], the CNO neutrino flux scales with the metal

abundance in the solar core, which probes the initial chemical composition of the Sun at its formation. The metal abundance in the core is decoupled from the surface by a radiative zone, and CNO neutrinos are the only probe of the initial condition.

Here we want to investigate if an energy window exists where precise measurement of the CNO flux can be performed in our low background module. We use our by-now standard simulation tools to count true deposited energy for a variety of backgrounds and solar neutrino sources in a 3 kTon fiducial volume. We impose a 2% energy smearing, as is reasonable by arguments in section 2.3.1. Fluxes come from [66] with a 0.3 survival probability applied, as appropriate to this low energy range (see figure 12). We use the assumption that the  $^{42}\text{Ar}$  content will be at a rate that is reduced by a further factor 100 000 compared to atmospheric argon. We emphasize again per section 2.2.3 this is likely very conservative. The result is we see in a window about 0.2 MeV wide just above the *pep* cutoff that the CNO signal sticks up above other solar neutrino sources. This is merely an illustration; a real analysis will likely do a templated fit above the  $^7\text{Be}$  peak. Neutrons from the cold cryoskin stainless steel are forced to be low, as usual; radon is taken as controlled. The  $^{210}\text{Bi}$  background which Borexino took exquisite care to control and measure [65] is yet to be thoroughly investigated here. Nevertheless, there would appear to be a window where the high and low metallicity solutions are statistically separable. By comparison, CNO sensitivity in the two-phase LArTPC program, which studies are further along than the current work, can be seen in [67].

*Triggering for CNO neutrinos.* Initial studies into measuring the CNO flux with TPC triggering are underway, taking into account the full complement of radiological backgrounds predicted in the DUNE detector. In these early studies, TPC triggering requires sufficiently large, coincident clusters on the collection plane and at least one induction plane. We expect future work will in fact lead to a much higher-efficiency, light-based trigger being implemented for most work discussed in this paper. The dominant background in the 1.4–2.0 MeV energy window is radon in this early TPC triggering study, not in fact solar neutrinos—despite the rate reduction by a factor of  $10^3$  predicted in the low background module. In order to perform the true CNO detection there is clearly much work to be done in offline processing to accurately characterize and implement rejection by alpha detection, Bi–Po coincidence, disproportionate activity near the cathode from drifting cation decay products, and emanation properties of the various detector materials.

*3.5.5. Precision measurement of hep flux.* The hep solar neutrino process ( $^3\text{He} + p \rightarrow ^4\text{He} + e^+ + \nu_e$ ) produces the highest energy neutrinos, though they have the lowest flux and have not yet been observed. This low background module will be able to measure tens of these neutrinos per year via CC events, with a significant reduction in the background due to radon and neutron interactions within the liquid argon.

### 3.6. Neutrinoless double beta decay

A discovery of neutrinoless double beta decay ( $0\nu 2\beta$ ) is the most straightforward way to prove the Majorana nature of neutrinos. It would be parsimonious to be able to search for  $0\nu 2\beta$  in the same detector we are suggesting to use for the other measurements mentioned in this paper.  $^{136}\text{Xe}$  is one isotope in which much work is being performed worldwide to try to make this discovery [68, 69].

Loading large LArTPCs with a few-percent level Xe and measuring neutrinoless double beta decay has been suggested in [70] and [71] among other places. In this subsection we show that naively a discovery is likely possible with a signal  $^{136}\text{Xe}$  half-life of  $5 \times 10^{28}$  years,

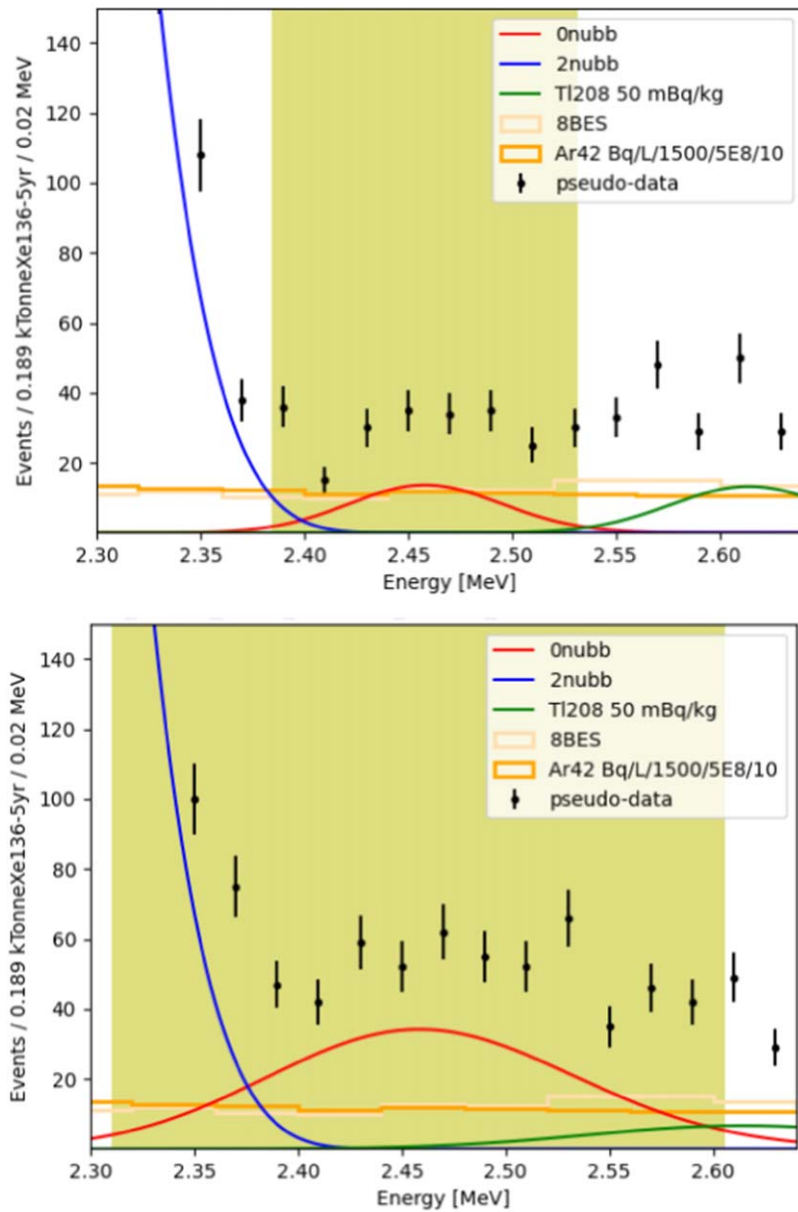


**Figure 13.** An optimistic background/resolution scenario for a  $^{136}\text{Xe}$   $0\nu\beta\beta$  half-life of  $5 \cdot 10^{28}$  years. Detector energy resolution is 1.5% on top. Backgrounds are as discussed in the text. On the bottom is the same with a reduced resolution of 3% and for a half-life of  $1 \cdot 10^{28}$  years.

and is quite apparent at  $1 \times 10^{28}$  years, provided energy resolution requirements can be met. We imagine, say, a five-year search campaign for  $0\nu\beta\beta$  at the end of the prosecution of the baseline physics program of this module, since any dark matter search requiring PSD would necessarily be compromised by xenon loading.

We start with a  $0\nu 2\beta$  signal calculated using a Gaussian 1.5 (3)% energy resolution at 2.435 MeV with  $1/\sqrt{E}$  dependence for top (bottom) plots in figure 13. Energy resolution ambitions are consistent [72] with what we may expect in a LArTPC from charge energy collection in combination with the photon readout system, as well as a discussion in section 2.3.1. We similarly smear the  $2\nu$  double beta true spectrum by these resolutions. And for the  $^{208}\text{Tl}$  background emanating from the G10 of the charge readout planes we use only the expected rate from the simulation, creating the actual spectrum by likewise smearing the 2.6 MeV gamma by 1.5 (3)% in the top (bottom) plots. For the solar and  $^{42}\text{Ar}$  backgrounds previously discussed, on the other hand, we use the resolution from the simulation that uses only the poorer light-only collection from the SiPM hits. These are flat backgrounds that extend to low energy where the signal will likely be obscured in the noise of the charge readout, hence the need to rely on only the SiPMs. For both plots we use a 3% concentration of  $^{136}\text{Xe}$  in our inner volume, using a 2.0 kTon fiducial volume, and propose to run for five years. We plot a signal corresponding to a  $(5)1 \times 10^{28}$  year  $0\nu\beta\beta$  half-life.

Among the assumptions made for our figures is that underground argon can give a  $^{42}\text{Ar}$  suppression of a factor of 10 beyond that in atmospheric Ar. See section 2.2.3 which indicates this is likely easily achievable, up to processing concerns. We also take in figure 13 that the irreducible solar  $^8\text{B}$  elastic scattering may be suppressed by a factor of two (conservatively down from three assumed in [73, 74]) from inspecting Cherenkov/Scintillation light ratios in single versus double electron events. We impose no efficiency hit due to this cut, whereas [73] uses an efficiency of 0.75. More careful event reconstruction studies are needed to bear out the reasonableness of this cut. We assign the  $^{208}\text{Tl}$  in the G10 charge collection planes a Th concentration of  $50 \text{ mBq kg}^{-1}$ . Charged current solar neutrino events, are in principle reducible to zero, due to the excited state gammas that are emitted. And similarly, neutrons shall be almost entirely removed using pulse shape discrimination. We again take the radon issue to be solved for the sake of this study. A  $2\sigma$  band to either side of the  $0\nu\beta\beta$  energy of 2.435 MeV is shown.

We take  $E_{\text{res}} \sim 1.5\%$  in the top plot at the Q-value, even though, as we have said, it is not immediately obvious we can achieve that (nor in fact are we currently confident we can reach the 2.5% of the bottom plot) with our charge readout plus 80% SiPM coverage, open as it is at the top and bottom. That study is beyond the scope of this paper. However, we see that there is sensitivity in this detector to  $0\nu\beta\beta$  discovery at lifetimes that stretch the reach of coming experiments, despite the large, irreducible solar  $^8\text{B}$  neutrinos which elastically scatter off the mostly argon target.

### 3.7. Dark matter

It is known that a large amount of dark matter exists within the Universe, that has so far only been observed by gravitation interactions. One popular candidate for the dark matter is the Weakly Interacting Massive Particle, or WIMP, that is, the focus of several current and future experiments. The potential of using this low background module to search for WIMP dark matter was studied in [10]. This study assumed a dual phase TPC design, with a single fiducial volume at the center of the detector (rather than the split fiducial volumes described above). The criteria for achieving a sensitive WIMP dark matter search was set as requiring:

- a 50–100 keV nuclear recoil threshold;
- $\mathcal{O}(10)$  background events;
- $\mathcal{O}(100)$  photons detected per event to allow pulse shape discrimination (PSD).



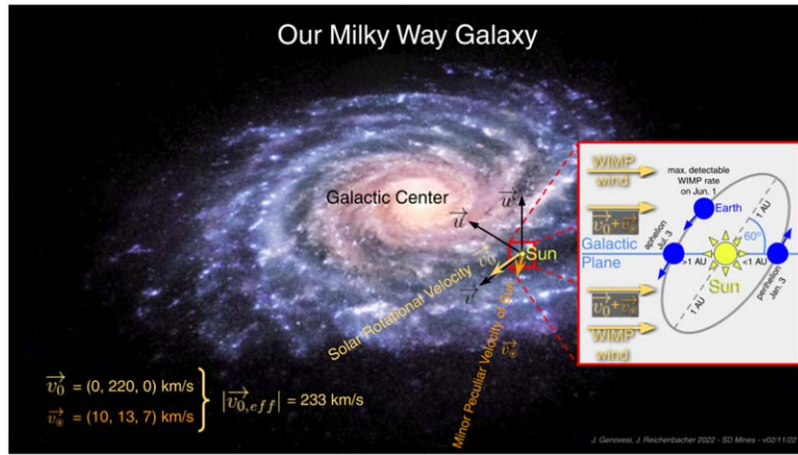


**Figure 14.** Galactic WIMP wind as it relates to Earth's orbital plane employing an illustrative rendition [79] of our Milky Way galaxy. Our solar systems velocity in reference to our galaxy has contributions from both a rotational aspect with a tangential velocity of  $220 \text{ km s}^{-1}$  and from a minor solar peculiar aspect with velocity components  $(U, V, W) = (10, 13, 7) \text{ km s}^{-1}$  [80]. In our model the combined relative velocity of our solar system is then  $233 \text{ km s}^{-1}$  at which the Sun moves through a gas-like halo of WIMP dark matter assumed to have a Maxwell-Boltzmann-like velocity distribution. This induces what we experience as a 'WIMP wind'. This WIMP wind is at an angle compared to Earth's rotation around the Sun as pictured in the zoomed-in diagram, with the effective WIMP velocity distribution shifted up when flowing maximally into the wind and shifted down when flowing maximally with the wind. Due to this aspect, an analysis of the annual modulation of detectable WIMP rate on Earth could provide a powerful tool for identifying the WIMP nature of dark matter.

Assuming that 1250 photons per 100 keV of prompt scintillation light is emitted (as measured by SCENE for  $500 \text{ V cm}^{-1}$  fields [75]), the studies in section 3.3 show that reaching 100 photons per event is realistic. A pseudo-Monte Carlo simulation of the Poisson distributed light output was performed to determine the width of a typical PSD variable  $f_{90}$ , defined as the ratio of the light detector detected in the first 90 ns of an event to the light detected in the second 90 ns of an event, for the  $^{39}\text{Ar}$  decays. The results are taken from measurements of the SCENE experiment [75]. Reference [10] shows PSD is expected to reach the  $10^{10}$  rejection level for electron/gamma backgrounds. We also direct the interested reader to the PSD study [76] to suppress the  $^{39}\text{Ar}$  decay background in DEAP.

All other electron/gamma backgrounds are expected to be subdominant to the  $^{39}\text{Ar}$  and will thus be removed by PSD. Neutron backgrounds were managed as described above. The main background will be from irreducible atmospheric neutrinos at the so-called neutrino floor. A full background table from the study is shown in [10].

The background rates are used to set a 90% C.L. sensitivity to WIMP dark matter [10] shows that a three-year search with this detector will have comparable sensitivity to planned next-generation detectors, which have expected run times of 10 years. This timescale allows a rapid cross-check of any signals discovered in these detectors, in particular for liquid argon experiments such as DarkSide-20k [9] or ARGO [77].

**3.7.1. Seasonal variation of rate for WIMP dark matter.** The prominent model for dark matter (DM) is the so-called Standard Halo Model (SHM) [78] featuring WIMP DM. The SHM

describes a basic isometric spherical distribution of WIMP DM around our galaxy and has been used due to it being a good trade-off between realism and simplicity. The relative velocity of our solar system of  $233 \text{ km s}^{-1}$  [79] at which the Sun moves through the gas-like halo of WIMP DM induces a WIMP wind. Figure 14 illustrates the Sun's rotation in our galaxy together with Earth's solar orbit into and out of the WIMP wind. We modeled the Sun's rotational and peculiar velocities into one combined effective velocity of  $233 \text{ km s}^{-1}$  in the galactic plane and accounted for the  $60^\circ$  inclined plane of Earth's orbit. We were then able to accurately describe the annual modulation of detectable WIMP rate  $R$  on Earth by one simple periodic sinusoidal function with one amplitude parameter  $A$  and a maximal rate on June 1 of each year [79, 80]:

$$R([\text{d}^{-1}]) = A [\text{d}^{-1}] \times \cos\left(\frac{2\pi}{T[\text{d}]} \times (t[\text{d}] - t_{\text{June1}}[\text{d}])\right) + R_{\text{avg}} [\text{d}^{-1}]. \quad (2)$$

The constant term  $R_{\text{avg}}$  is the average annual rate. Earth's period  $T$  is 365.2422 d and the phase corresponding to the maximal rate  $R_{\text{max}}$  observable on June 1 of each year is  $2\pi \cdot t_{\text{June1}}/T = 2\pi \cdot 0.415$ .

Galactic WIMPs in the halo are assumed to have a Maxwell–Boltzmann-like velocity distribution. The effective WIMP velocity distribution is shifted up when Earth is flowing maximally into the WIMP wind and shifted down when Earth is flowing maximally with the WIMP wind. Due to this aspect, an analysis of the annual modulation of the detection rate  $R$  could provide a powerful tool for identifying WIMP DM. Due to the unrivaled large fiducial mass of 3 kTons and a potentially very long DUNE operation of one decade (or even several), this concept can offer a unique detection of the seasonal variation of the detectable WIMP rate  $R$  at a sufficient statistical significance for providing a smoking gun signature for the WIMP nature of DM. This would be particularly of interest in case upcoming generation-2 DM experiments like LZ [81] and/or XENONnT [82] have evidence for WIMPs near their sensitivity. It would be nearly impossible for the planned generation-3 DM experiments [83, 84] to make such a smoking gun detection proving the WIMP nature of DM.

The differential rate of interactions in an arbitrary detector for the SHM is described in equation (3):

$$\frac{dR}{dE_R} = \sigma_N^{\text{SI}} \frac{A^2 m_A N_T \rho_\chi}{2m_\chi \mu_N^2} F^2(E_R) \int_{\nu_{\min}(E_R)}^{\infty} \frac{d^3 \vec{\nu}}{\nu} f_{\oplus}(\vec{\nu}, \vec{\nu}_{\text{obs}}), \quad (3)$$

where  $\sigma_N^{\text{SI}}$  is the spin-independent-nucleon cross-section for WIMPs,  $A$  is the atomic number of argon,  $m_A$  is the mass of argon,  $N_T$  is the number of target nuclei,  $\rho_\chi$  is the local dark matter density ( $0.3 \frac{\text{GeV}}{\text{cm}^3}$ ),  $m_\chi$  is the mass of a WIMP,  $\mu_N$  is the reduced WIMP-nucleus mass,  $F(E_R)$  is the nuclear form-factor,  $\nu_{\min}$  is minimum WIMP velocity to produce a recoil of energy  $E_R$ ,  $\nu$  is WIMP velocity, and  $\nu_{\text{obs}}$  is the observer velocity with respect to the Galaxy. When Earth is moving into or with the WIMP wind, it affects the differential WIMP rate, which in turn would affect our  $\vec{\nu}_{\text{obs}}$ . For ease, we can define:

$$\int_{\nu_{\min}(E_R)}^{\infty} \frac{d^3 \vec{\nu}}{\nu} f_{\oplus}(\vec{\nu}, \vec{\nu}_{\text{obs}}) = \zeta(E_R), \quad (4)$$

where

$$f(\vec{\nu}) = \frac{1}{N} \left( e^{-\frac{\nu^2}{v_0^2}} - e^{-\frac{\nu_{\text{esc}}^2}{v_0^2}} \right), \quad (5)$$

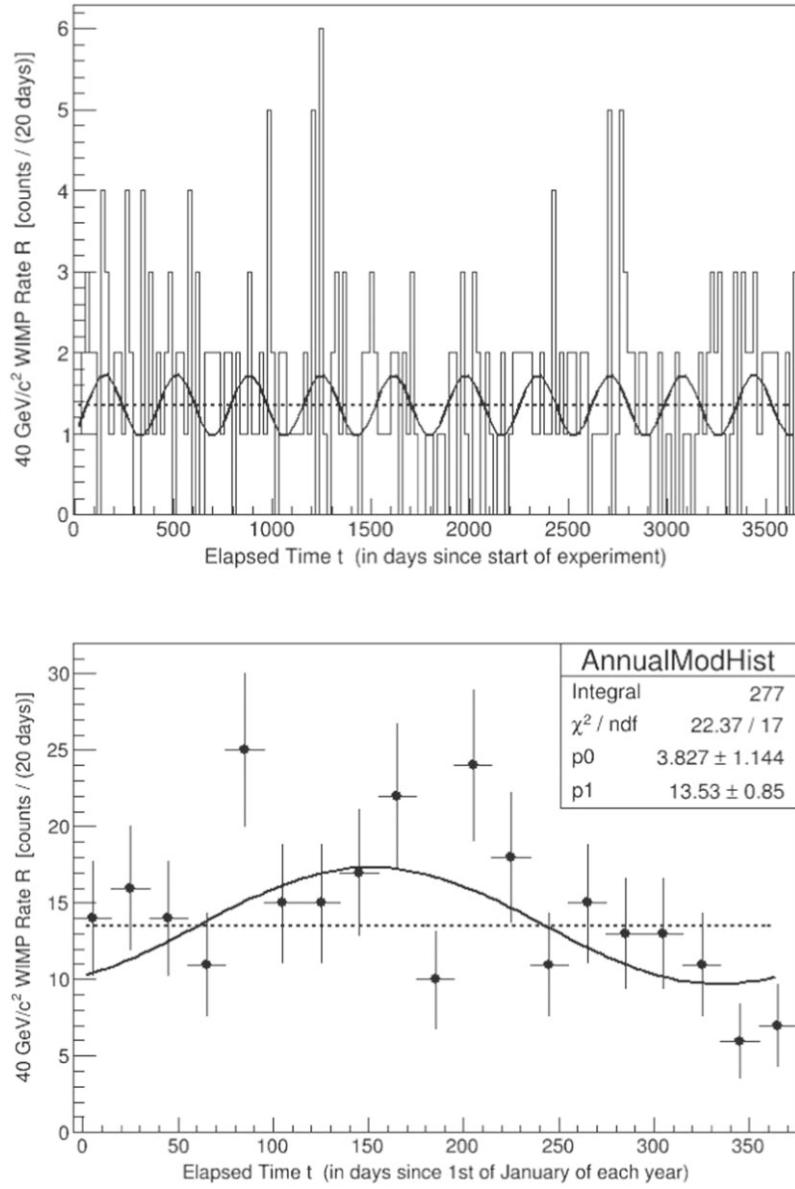


**Figure 15.** Example NEST [85] simulation of the annual modulation for 40 GeV/c<sup>2</sup> WIMP dark matter with a cross-section of  $4 \times 10^{-48} \text{ cm}^2$  for a 10 year measurement time with 3 kTon LAr at 50 keV threshold. On top, a Likelihood-fit result for a 10 year period and on the bottom the same data combined into a single annual period starting on January 1 of each year fitted with a  $\chi^2$ -method. The ideal case without background is assumed in this study.

and

$$f_{\oplus}(\vec{\nu}, \vec{\nu}_{\text{obs}}) = f(\vec{\nu} + \vec{\nu}_{\text{obs}}) \quad (6)$$

with  $N$  as a normalization factor,  $\nu_0$  is the expected WIMP velocity, and  $\nu_{\text{esc}}$  is the escape velocity of the Galaxy. Using equation (5), we can solve for individual cases of WIMPs in certain speed brackets.

As mentioned earlier, Earth’s orbit can play a crucial role in differential WIMP rate predictions in the SHM. As the solar system travels through our galaxy, observers on Earth would observe WIMPs dominantly from a certain direction in a windshield-to-rain like effect. This is due to the distribution of WIMPs being treated as a gas with a Maxwell–Boltzmann-like velocity distribution with the stars in our galaxy moving through the dark matter due to their orbits around the galactic nucleus. In addition to the standard rotational contribution from the solar system, a minor peculiar velocity exists in our solar system traveling through the Galaxy. This WIMP wind would be at an angle of  $60^\circ$  towards Earth’s orbital plane. This means that on June 1, the Earth will experience a maximum effective flux of WIMPs while on December 1 the Earth will have experienced the lowest effective WIMP rate, as one can see again in figure 14.

An example fit using equation (2) of an annual modulation signal simulated in NEST [85] without background is shown in figure 15 on top for a 10 year period, and on the bottom the same data combined into a single annual period starting on January 1 of each year. This is for a  $40 \text{ GeV}/c^2$  WIMP with a cross-section of  $4 \times 10^{-48} \text{ cm}^2$ , which is very close to the limit of sensitivity of the upcoming generation-2 xenon dark matter experiments LZ [81] and XENONnT [82]. We further assumed a  $3 \text{ kTon} \times 10 \text{ year}$  exposure of our proposed low background LAr module with a 50 keV threshold resulting in 277 events. The bottom plot of figure 15 shows a good  $\chi^2$ -fit result for the amplitude  $A = 3.827 \pm 1.144$  from equation (2). It confirms the possible measurement of the seasonal variation of the WIMP rate at a sufficient statistical significance for providing a smoking gun signature for the WIMP nature of DM. This will be uniquely possible with this detector, due to the unrivaled large mass of 3 kTons versus only 300 tons of argon for ARGO [84] and 100 tons for a Gen-3 xenon experiment [83]. Moreover, the annual modulation effect in xenon is significantly smaller due to the relatively lower energies of nuclear recoils in xenon compared to argon. Last but not the least, the logistics of a decade-long operation with this detector can utilize strong synergies with the DUNE long-baseline physics, including the cavern availability and occupancy.

### 3.8. Additional topics

This module, with its unprecedented combination of low background and size, also can explore several other topics. We describe several examples in this section.

**3.8.1. Atmospheric neutrinos.** The detector will measure approximately 10 CE $\nu$ NS events due to atmospheric neutrinos. These events have not yet been observed and this would allow a cross-check of background rates from the upcoming generation of dark matter experiments.

**3.8.2. Strangelets.** Recently, the paper ‘Can strangelets be detected in a large LAr neutrino detector?’ [86], predicted that a LArTPC detector is able to detect and discriminate light strangelets with  $(Z, A)$  between  $(2, 14)$  and  $(7, 70)$  for energies up to 10 GeV in the presence of radioactive background found at the surface. When operated underground the detection limits are expected to be extended due to lower background levels and, combined with the increased dimensions of the detector module, will improve the event rates by a factor of 40. In the case of strangelets, the main uncertainties are due to the estimations of their survival probability deep underground. The presence of  $^{39}\text{Ar}$  masks both ionization and scintillation

signals from strangelets and induces false signals in the collected charge from ionization. The use of underground argon in this module allows a cleaner detection signal.

*3.8.3. Charged micro-black holes and superheavy dark matter.* Hawking [87] suggested that unidentified tracks in the photographs taken in old bubble chamber detectors could be explained as signals of gravitationally ‘collapsed objects’ ( $\mu$ BH). The small black holes are expected to be unstable due to Hawking radiation, but the evaporation is not well-understood at masses of the order of the Planck scale. Certain inflationary models naturally assume the formation of a large number of small black holes [88] and the generalized uncertainty principle may indeed prevent total evaporation of small black holes by dynamics and not by symmetry, just like the hydrogen atom is prevented from collapse by the standard uncertainty principle [89]. Given the profound nature of the issues addressed, some disagreement and controversy exist.

In principle the direct detection of charged micro-black holes with masses around and upward of the Planck scale ( $10^{-5}$  g), ensuring a classical gravitational treatment of these objects, is possible in huge LAr detectors. It has been shown that the signals (ionization and scintillation) produced in LAr enable the discrimination between micro-black holes (with masses between  $10^{-5}$  and  $10^{-4}$  grams, and velocities in the range 250–1000 km s<sup>-1</sup>) and other particles [90]. It is expected that the trajectories of these micro-black holes will appear as crossing the whole active medium, in any direction, producing uniform ionization and scintillation on the whole path.

Along these lines, an analysis looking for multiple co-linear nuclear recoils can also probe ultra-heavy dark matter beyond the Planck scale, as described in [91, 92]. Sensitivity to the heaviest dark matter candidates is limited by the number density of the dark matter, which is inversely proportional to the mass, as the ability to detect heavy dark matter with a high cross section is set by the probability that a dark matter particle enters the detector. As such, sensitivity to the highest masses scales with the detector’s surface area, and would leverage the large size of this module compared to DEAP-3600, which has a 1.7 m diameter.

Similarly, in the direct detection of the charged micro-black holes, unlike in traditional WIMP detection, there will exist both ionization and scintillation signals from direct interactions and from recoiling nuclei. The capability to perform pulse shape discrimination in this detector will allow these tracks to be identified. Natural radioactivity is the main source of background in this case and the reduced number of free electrons (and photons) from beta decays of <sup>39</sup>Ar will allow a significant improvement of the capability of the detector to correctly identify the micro-black-hole signals.

*3.8.4. Other topics.* This detector would have sensitivity to a small number of CE $\nu$ NS events within the neutrino beam. It may have applications to geologic tomography. The improved energy resolution for low energy could have applications in searches for other exotics and beyond the standard model physics phenomena. Though the optimal search region for a diffuse supernova neutrino background is above the energy of the solar neutrinos [93], and thus the radioactive backgrounds, the improved energy resolution of this detector will again likely improve the search sensitivity.

## 4. Conclusion

We have presented a design in this paper for a low background kTon-scale LArTPC to potentially expand the current physics program for such detectors. The design is based on the

vertical drift detector planned for DUNE's second far detector module. The module discussed is a candidate for a third or fourth DUNE 'Module of Opportunity.' It is realized by providing additional shielding, stringent radioactive background control and enhanced light detection to the nominal vertical drift module. Energy resolution will benefit in all energy ranges due to event reconstruction and topology classification improvements from the superior light detection system and the quiet detector, which will allow to capture more cascade gammas [13] and thereby improve the hadronic component of neutrino–nucleus interactions.

The physics goals achieved by the SLoMo design extend the capability of large LArTPCs to search for solar and supernova neutrinos, neutrinoless double beta-decay, and WIMP dark matter. At the same time the design proposed here, by the nature of its small perturbations to the vertical drift module, assures continuing strong support to the long-baseline neutrino oscillation program to measure the remaining parameters in the PMNS matrix.

## **Acknowledgments**

Pacific Northwest National Laboratory (PNNL) is operated by Battelle for the United States Department of Energy (DOE) under Contract No. DE-AC05-76RL01830. Parts of this study at PNNL were supported by the DOE, USA Office of High Energy Physics Advanced Technology R&D subprogram and other parts by the Open Call Initiative, under the Laboratory Directed Research and Development Program. In the United Kingdom, this work was supported by STFC. For IL and MP, this work was performed with the financial support of the Romanian Program PNCDI III, Programme 5, Module CERN-RO, under contract no. 04/2022. KS is supported by the Department of Energy and the National Science Foundation. ZD acknowledges the support of the U.S. Department of Energy Office of Science under contract number DE- AC02-06CH11357. South Dakota School of Mines and Technology acknowledges the support of the Department of Energy through award number DE-SC0014223, as well as DE-AC02-07CH11359 through a sub-award from Fermi National Accelerator Laboratory subcontract No. 664706. JZ gratefully acknowledges using the resources of the Fermi National Accelerator Laboratory (Fermilab), a U.S. Department of Energy, Office of Science, HEP User Facility. Fermilab is managed by Fermi Research Alliance, LLC (FRA), acting under Contract No. DE-AC02-07CH11359.

## **Data availability statement**

The data cannot be made publicly available upon publication because they are not available in a format that is sufficiently accessible or reusable by other researchers. The data that support the findings of this study are available upon reasonable request from the authors.

## **ORCID iDs**

E Church <https://orcid.org/0000-0002-0155-5812>

C M Jackson <https://orcid.org/0000-0001-8096-6187>

M Parvu <https://orcid.org/0000-0002-6118-5251>

## References

- [1] Abi B *et al* (DUNE Collaboration) 2020 Deep Underground Neutrino Experiment (DUNE), Far Detector Technical Design Report, vol 4: Far Detector Single-phase Technology arXiv:2002.03010
- [2] Abud A A *et al* (DUNE Collaboration) 2022 Design, construction and operation of the ProtoDUNE-SP liquid argon TPC *J. Instrum.* **17** P01005
- [3] Amerio S *et al* (ICARUS Collaboration) 2004 Design, construction and tests of the ICARUS T600 detector *Nucl. Inst. Methods A* **527** 329–410
- [4] Qian X *et al* Snowmass 2021 letter of interest: development of LArTPC vertical drift solutions with PCB anode readouts for DUNE [https://www.snowmass21.org/docs/files/summaries/NF/SNOWMASS21-NF10\\_NF0-IF9\\_IF8\\_Xin\\_Qian-123.pdf](https://www.snowmass21.org/docs/files/summaries/NF/SNOWMASS21-NF10_NF0-IF9_IF8_Xin_Qian-123.pdf)
- [5] Best A, Görres J, Junker M, Kratz K-L, Laubenstein M, Long A, Nisi S, Smith K and Wiescher M 2016 Low energy neutron background in deep underground laboratories *Nucl. Instrum. Methods Phys. Res. A* **812** 1–6
- [6] Zhu G, Li S W and Beacom J F 2019 Developing the MeV potential of DUNE: detailed considerations of muon-induced spallation and other backgrounds *Phys. Rev. C* **99** 055810
- [7] Capozzi F, Li S W, Zhu G and Beacom J F 2019 DUNE as the next-generation solar neutrino experiment *Phys. Rev. Lett.* **123** 131803
- [8] Reichenbacher J 2021 ( $\alpha$ , n) cross section data improvement needs for next generation low-background neutrino and dark matter experiments *IAEA Technical Meeting on ( $\alpha$ ,n) Nuclear Data Evaluation and Data Needs, Vienna*
- [9] Aalseth C E *et al* 2018 DarkSide-20k: a 20 tonne two-phase LAr TPC for direct dark matter detection at LNGS *Eur. Phys. J. Plus* **133** 131
- [10] Church E, Jackson C M and Saldanha R 2020 Dark matter detection capabilities of a large multipurpose liquid argon time projection chamber *J. Instrum.* **15** P09026
- [11] Stock J and Reichenbacher J 2017 Radiopurity screening and radiological model for DUNE *Conf. on Science at the Sanford Underground Research Facility (CoSSURF) (Rapid City, SD)*
- [12] Reichenbacher J and for the (DUNE Collaboration) 2017 Supernova neutrinos, proton decay and atmospheric neutrinos at DUNE *26th Int. Workshop on Weak Interactions and Neutrinos (WIN 2017)*
- [13] Caratelli D *et al* 2022 Low-energy physics in neutrino LArTPCs arXiv:2203.00740
- [14] Aalseth C E *et al* 2018 DarkSide-20k: a 20 tonne two-phase LAr TPC for direct dark matter detection at LNGS *Eur. Phys. J. Plus* **133** 131
- [15] Ajaj R *et al* (DEAP Collaboration) 2019 Search for dark matter with a 231 day exposure of liquid argon using DEAP-3600 at SNOLAB *Phys. Rev. D* **100** 022004
- [16] Aprile E *et al* (XENON Collaboration) 2017 Online  $^{222}\text{Rn}$  removal by cryogenic distillation in the XENON100 experiment *Eur. Phys. J. C* **77** 358
- [17] Pushkin K *et al* 2018 Study of radon reduction in gases for rare event search experiments *Nucl. Instrum. Methods Phys. Res. A* **903** 267–76
- [18] Heusser G, Rau W, Freudiger B, Laubenstein M, Balata M and Kirsten T 2000  $^{222}\text{Rn}$  detection at the  $\mu\text{Bq}/\text{m}^3$  range in nitrogen gas and a new Rn purification technique for liquid nitrogen *Appl. Radiat. Isot.* **52** 691–5
- [19] Abratenko P *et al* (The MicroBooNE collaboration) 2022 Observation of radon mitigation in MicroBooNE by a liquid argon filtration system *J. Instrum.* **17** P11022
- [20] Pocar A 2005 Low background techniques for the Borexino nylon vessels *AIP Conf. Proc.* **785** [http://works.bepress.com/andrea\\_pocar/](http://works.bepress.com/andrea_pocar/)
- [21] Akerib D S *et al* 2020 The LUX-ZEPLIN (LZ) radioactivity and cleanliness control programs *Eur. Phys. J. C* **80** 1044 C
- [22] Street J, Bunker R, Miller E H, Schnee R W, Snyder S and So J 2018 Radon mitigation for the SuperCDMS SNOLAB dark matter experiment *AIP Conf. Proc.* **1921** 050002
- [23] National Nuclear Data Center <https://nndc.bnl.gov/nudat3/>.
- [24] Benetti P *et al* 2007 Measurement of the specific activity of  $^{39}\text{Ar}$  in natural argon *Nucl. Instrum. Methods Phys. Res. A* **574** 83–8
- [25] Mei D-M, Yin Z-B, Spaans J, Koppang M, Hime A, Keller C and Gehman V M 2010 Prediction of underground argon content for dark matter experiments *Phys. Rev. C* **81** 055802
- [26] Agnes P *et al* 2016 Results from the first use of low radioactivity argon in a dark matter search *Phys. Rev. D* **93** 081101

- [27] Nowak J *et al* (Darkside Collaboration) 2021 Separating  $^{39}\text{Ar}$  from  $^{40}\text{Ar}$  by cryogenic distillation with Aria for dark matter searches *Eur. Phys. J. C* **81** 359
- [28] Barabash A S, Saakyan R R and Umatov V I 2016 On concentration of  $^{42}\text{Ar}$  in liquid argon *J. Phys. Conf. Ser.* **718** 062004
- [29] Peurrung A J, Bowyer T W, Craig R A and Reeder P L 1997 Expected atmospheric concentration of  $^{42}\text{Ar}$  *Nucl. Instrum. Methods Phys. Res. A* **396** 425–6
- [30] Cennini P *et al* 1995 On atmospheric  $^{39}\text{Ar}$  and  $^{42}\text{Ar}$  abundance *Nucl. Instrum. Methods Phys. Res. A* **356** 526–9
- [31] Rumble J R 2020 *Handbook of Chemistry and Physics* (New York: CRC Press)
- [32] Lubashevskiy A *et al* 2018 Mitigation of  $^{42}\text{Ar}/^{42}\text{K}$  background for the GERDA Phase II experiment *Eur. Phys. J. C* **78** 15
- [33] Schröder J, Münnich K O and Ehhalt D H 1971 Physical sciences: Krypton-85 in the troposphere *Nature* **233** 614–5
- [34] DEAP Collaboration, Adhikari P 2019 Electromagnetic backgrounds and potassium-42 in the DEAP-3600 dark matter detector *Phys. Rev. D* **100** 072009
- [35] Renshaw A 2018 Procuring 50 tonnes of underground argon for DS-20k (<https://doi.org/10.5281/zenodo.1239080>)
- [36] Saldanha R, Back H O, Tsang R H M, Alexander T, Elliott S R, Ferrara S, Mace E, Overman C and Zalavadia M 2019 Cosmogenic production of  $^{39}\text{Ar}$  and  $^{37}\text{Ar}$  in argon *Phys. Rev. C* **100** 024608
- [37] Zhang C and Mei D 2022 Evaluation of cosmogenic production of  $^{39}\text{Ar}$  and  $^{42}\text{Ar}$  for rare-event physics using underground argon *Astroparticle Physics* **142** 102733
- [38] Saldanha R, Back H O, Tsang R H M, Alexander T, Elliott S R, Ferrara S, Mace E, Overman C and Zalavadia M 2019 Cosmogenic production of  $^{39}\text{Ar}$  and  $^{37}\text{Ar}$  in argon *Phys. Rev. C* **100** 024608
- [39] Parvu M and Lazanu I 2021 Radioactive background for ProtoDUNE detector *J. Cosmol. Astropart. Phys.* JCAP08(2021)042
- [40] Zhang C and Mei D-M 2022 Evaluation of cosmogenic production of  $^{39}\text{Ar}$  and  $^{42}\text{Ar}$  for rare-event physics using underground argon *Astropart. Phys.* **142** 102733
- [41] Szydagis M *et al* 2021 A Review of basic energy reconstruction techniques in liquid xenon and argon detectors for dark matter and neutrino physics using NEST *Instruments* **5** 13
- [42] Bhat A 2021 MeV scale physics in MicroBooNE *PhD Thesis* Syracuse U.
- [43] Jones B J P, Chiu C S, Conrad J M, Ignarra C M, Katori T and Toups M 2013 A measurement of the absorption of liquid argon scintillation light by dissolved nitrogen at the part-per-million level *J. Instrum.* **8** P07011
- [44] Agostinelli S *et al* 2003 Geant4—a simulation toolkit *Nucl. Instrum. Methods Phys. Res.* **506** 250–303 A
- [45] Church E 2020 Large-LArTPC-Optical Monte Carlo Code [https://github.com/echurch/rdecay02/tree/liquid\\_deception](https://github.com/echurch/rdecay02/tree/liquid_deception)
- [46] Totani T, Sato K, Dalhed H E and Wilson J R 1998 Future detection of supernova neutrino burst and explosion mechanism *Astrophys. J.* **496** 216–25
- [47] Gardiner S 2021 Nuclear de-excitations in low-energy charged-current  $\nu_e$  scattering on  $^{40}\text{Ar}$  *Phys. Rev. C* **103** 044604
- [48] Abi B *et al* 2021 Supernova neutrino burst detection with the deep underground neutrino experiment *Eur. Phys. J. C* **81** 423
- [49] Li S W, Roberts L F and Beacom J F 2021 Exciting prospects for detecting late-time neutrinos from core-collapse supernovae *Phys. Rev. D* **103** 023016
- [50] Odrzywolek A, Misiaszek M and Kutschera M 2004 Detection possibility of the pair—annihilation neutrinos from the neutrino—cooled pre-supernova star *Astropart. Phys.* **21** 303–13
- [51] Odrzywolek A, Misiaszek M and Kutschera M 2004 Neutrinos from pre-supernova star *Acta Phys. Polon. B* **35** 1981
- [52] Odrzywolek A and Heger A 2010 Neutrino signatures of dying massive stars: from main sequence to the neutron star *Acta Phys. Polon. B* **41** 1611–28
- [53] Kato C, Nagakura H, Furusawa S, Takahashi K, Umeda H, Yoshida T, Ishidoshiro K and Yamada S 2017 Neutrino emissions in all flavors up to the pre-bounce of massive stars and the possibility of their detections *Astrophys. J.* **848** 48



- [54] Patton K M, Lunardini C and Farmer R J 2017 Presupernova neutrinos: realistic emissivities from stellar evolution *Astrophys. J.* **840** 2
- [55] Patton K M, Lunardini C, Farmer R J and Timmes F X 2017 Neutrinos from beta processes in a presupernova: probing the isotopic evolution of a massive star *Astrophys. J.* **851** 6
- [56] Mukhopadhyay M, Lunardini C, Timmes F X and Zuber K 2020 Presupernova neutrinos: directional sensitivity and prospects for progenitor identification *Astrophys. J.* **899** 153
- [57] Freedman D Z 1974 Coherent effects of a weak neutral current *Phys. Rev. D* **9** 1389–92
- [58] Kopeliovich V B and Frankfurt L L 1974 Isotopic and chiral structure of neutral current *JETP Lett. (USSR) (Engl. Transl.)* **19** 145–7
- [59] Akimov D (COHERENT Collaboration) *et al* 2021 First measurement of coherent elastic neutrino–nucleus scattering on argon *Phys. Rev. Lett.* **126** 012002
- [60] Kate S 2018 The CEvNS glow from a supernova (<https://doi.org/10.5281/zenodo.3464639>)
- [61] Esteban I, Gonzalez-Garcia M C, Maltoni M, Martinez-Soler I and Salvado J 2018 Updated constraints on non-standard interactions from global analysis of oscillation data *J. High Energy Phys.* JHEP08(2018)180
- Esteban I, Gonzalez-Garcia M C, Maltoni M, Martinez-Soler I and Salvado J 2020 Updated constraints on non-standard interactions from global analysis of oscillation data *J. High Energy Phys.* JHEP12(2020)152
- [62] Reichenbacher J and Sinev G 2022 NSI searches with current and future neutrino and dark-matter experiments Submitted for publication
- [63] Friedland A, Lunardini C and Pena-Garay C 2004 Solar neutrinos as probes of neutrino matter interactions *Phys. Lett. B* **594** 347–54
- [64] Friedland A, Gaesser M L, Shoemaker I M and Vecchi L 2012 Probing nonstandard standard model backgrounds with LHC monojets *Phys. Lett. B* **714** 267–75
- [65] BOREXINO Collaboration 2020 Experimental evidence of neutrinos produced in the CNO fusion cycle in the Sun *Nature* **587** 577–82
- [66] Vinyoles N, Serenelli A M, Villante F L, Basu S, Bergström J, Gonzalez-Garcia M C, Maltoni M, Peña-Garay C and Song N 2017 A new generation of standard solar models *Astrophys. J.* **835** 202
- [67] Franco D *et al* 2016 Solar neutrino detection in a large volume double-phase liquid argon experiment *J. Cosmol. Astropart. Phys.* JCAP08(2016)017
- [68] nEXO Collaboration *et al* 2018 *nEXO Pre-Conceptual Design Report* arXiv:1805.11142
- [69] NEXT Collaboration *et al* 2021 Sensitivity of a tonne-scale NEXT detector for neutrinoless double beta decay searches arXiv:2005.06467
- [70] Zennaro J, Psihas F and Mastbaum A Snowmass 2021 letter of interest: DUNE-Beta: searching for neutrinoless double beta decay with a large LArTPC [https://snowmass21.org/docs/files/summaries/NF/SNOWMASS21-NF5\\_NF10-IF8\\_IF0\\_Zennaro-175.pdf](https://snowmass21.org/docs/files/summaries/NF/SNOWMASS21-NF5_NF10-IF8_IF0_Zennaro-175.pdf)
- [71] Zennaro J, Mastbaum A and Psihas F 2022 Xenon-doped liquid argon TPCs as a neutrinoless double beta decay platform *Phys. Rev. D* **106** 092002
- [72] Foreman W *et al* 2020 Calorimetry for low-energy electrons using charge and light in liquid argon *Phys. Rev. D* **101** 012010
- [73] Brodsky J P, Sangiorgio S, Heffner M and Stiegler T 2019 Background discrimination for neutrinoless double beta decay in liquid xenon using Cherenkov light *Nucl. Instrum. Meth. A* **922** 76–83
- [74] Avasthi A *et al* 2021 Kiloton-scale xenon detectors for neutrinoless double beta decay and other new physics searches *Phys. Rev. D* **104** 112007
- [75] Cao H *et al* 2015 Measurement of scintillation and ionization yield and scintillation pulse shape from nuclear recoils in liquid argon *Phys. Rev. D* **91** 092007
- [76] Adhikari P and (DEAP Collaboration) 2021 Pulse-shape discrimination against low-energy Ar-39 beta decays in liquid argon with 4.5 tonne-years of DEAP-3600 data *Eur. Phys. J. C* **81** 823
- [77] Giovanetti G K and The Global Argon Dark Matter Collaboration Snowmass 2021 letter of interest: Searching for dark matter with liquid argon 2021 [https://snowmass21.org/docs/files/summaries/CF/SNOWMASS21-CF1\\_CF0\\_Giovanetti-172.pdf](https://snowmass21.org/docs/files/summaries/CF/SNOWMASS21-CF1_CF0_Giovanetti-172.pdf)
- [78] McCabe C 2010 Astrophysical uncertainties of dark matter direct detection experiments *Phys. Rev. D* **82** 023530
- [79] Reichenbacher J and Genovesi J 2021 Illustration and developed model of seasonal variation of detection rate of WIMP dark matter for simulations using NEST Private Communication

- [80] Savage C, Freese K and Gondolo P 2006 Annual modulation of dark matter in the presence of streams *Phys. Rev. D* **74** 043531
- [81] Akerib D S *et al* 2020 Projected WIMP sensitivity of the LUX-ZEPLIN dark matter experiment *Phys. Rev. D* **101** 052002
- [82] Aprile E *et al* 2020 Projected WIMP sensitivity of the XENONnT dark matter experiment *J. Cosmol. Astropart. Phys.* **JCAP11(2020)031**
- [83] Aalbers J *et al* 2023 A next-generation liquid xenon observatory for dark matter and neutrino physics *Journal Phys. G* **50** 013001
- [84] Bottino B 2022 DarkSide-20k and the future liquid argon dark matter program *PoS EPS-HEP2021* 169
- [85] Szydagis M *et al* 2021 A review of basic energy reconstruction techniques in liquid xenon and argon detectors for dark matter and neutrino physics using NEST *Instruments* **5** 13
- [86] Parvu M and Lazanu I 2021 Can strangelets be detected in a large LAr neutrino detector? *J. Cosmol. Astropart. Phys.* JCAP11(2021)040
- [87] Hawking S 1971 Gravitationally collapsed objects of very low mass *Mon. Not. Roy. Astron. Soc.* **152** 75
- [88] Chen P 2005 Inflation induced Planck-size black hole remnants as dark matter *New Astron. Rev.* **49** 233–9
- [89] Adler R J, Chen P and Santiago D I 2001 The Generalized uncertainty principle and black hole remnants *Gen. Rel. Grav.* **33** 2101–8
- [90] Lazanu I, Lazanu S and Pârnu M 2020 About detecting very low mass black holes in LAr detectors *J. Cosmol. Astropart. Phys.* **JCAP11(2021)040**
- [91] Adhikari P *et al* 2022 First direct detection constraints on planck-scale mass dark matter with multiple-scatter signatures using the DEAP-3600 detector *Phys. Rev. Lett.* **128** 011801
- [92] Carney D *et al* 2022 Snowmass 2021 cosmic frontier white paper: ultraheavy particle dark matter arXiv:2203.06508
- [93] MØller K, Suliga A M, Tamborra I and Denton P B 2018 Measuring the supernova unknowns at the next-generation neutrino telescopes through the diffuse neutrino background *J. Cosmol. Astropart. Phys.* **JCAP05(2018)066**